

The Migration of Giant Planets in Massive Protoplanetary Discs

Kate E. M. Robinson

A thesis submitted in partial fulfilment for the requirements for the degree
of *Master of Science* at the University of Central Lancashire.

Declaration

I declare that while registered as a candidate for the research degree, I have not been a registered candidate or enrolled student for another award of the University or other academic or professional institution. I declare that no material contained in the thesis has been used in any other submission for an academic award and is solely my own work.

Kate E. M. Robinson

July 2016

Abstract

If giant planets form by disc fragmentation early on during disc evolution, then they interact with the gas in the disc and as a result they will likely migrate, i.e. drift inwards or outwards. This study aims to explore the migration patterns of giant planets in unstable discs using radiative hydrodynamic simulations. More specifically we examine the migration of planets within different mass discs and at different orbital radii. We find that planets initially migrate inwards quickly. They are able to open up a gap and the migration stops and turns to a slow outward migration. Therefore, planets forming early on are able to survive on wide orbits. However, many of these planets accrete enough mass to become brown dwarfs. This could explain the observations of giant planets at wide orbital radii from the host star.

Contents

Contents	iv
List of Figures	vi
List of Tables	xii
1. Introduction	1
1.1 The Formation of the Disc	1
1.2 The Formation of the Planets.....	3
1.2.1 The Core Accretion Model.....	3
1.2.2 Gravitational Fragmentation.....	4
1.3 The Migration of Planets.....	5
1.3.1 Type I Migration.....	5
1.3.2 Type II Migration.....	6
1.4 Thesis Outline.....	8
2. Smoothed Particle Hydrodynamics	9
2.1 Introduction	9
2.2 Smoothing Kernels	10
2.3 Time Steps	11
2.4 The Barnes – Hut Tree	12
2.5 Sink Particles	12
2.6 The SEREN SPH Code	13
3. Setting Up the Disc Initial Conditions	14
3.1 Introduction	14

3.2 Disc Surface Density and Mass	14
3.3 Disc Temperature Profile	16
3.4 Disc Vertical Density Profile and Disc Thickness	16
3.5 Disc Velocity Profile	18
3.6 Setting Up the Positions of the SPH Particles	19
3.7 Setting Up the Smoothing Length of the SPH Particles	20
3.8 Summary	21
4. Testing the Code	22
4.1 Disc Setup	22
4.1.1 Disc Surface Density Profile	23
4.1.2 Temperature Profile	23
4.2 Relaxing the Disc	23
4.3 Comparing Simulations	24
4.4 Migration	26
4.5 Eccentricity	27
4.6 Accretion	27
4.7 Comparison with Ayliffe & Bate (2010)	28
4.8 Summary	29
5. Giant Planet Migration in Massive Discs	30
5.1 Setting Up the Discs	30
5.2 Planet Migration Within a $0.1M_{\odot}$ Disc	32
5.2.1 Surface Density	32
5.2.2 Migration Within the $0.1M_{\odot}$ Disc	33
5.2.3 Eccentricities of Planets within the $0.1M_{\odot}$ Disc	34
5.3 Planet Migration Within the $0.01M_{\odot}$ Disc	36
5.4 Comparison of the Simulations of Planet Migration in Massive Discs	41
5.5 Comparisons with Other Studies	47
5.6 Summary	48
6. Conclusions	49
References	51

List of Figures

- 1.1:** **Figure 1.1:** (a) Left: An example of a low mass, flared disc as seen edge-on. (b) Right: An example of a less flared, more massive disc. As the mass of the disc is proportional to the mass of the star at its centre, a more massive disc with a more massive star will not only have the increased self-gravity giving it a less flared profile but also will have a greater vertical component of the star's gravity pulling it towards the mid-plane. **Page 2**
- 1.2:** **Figure 1.2:** A diagram showing how accretion occurs due to accretion columns close to the star, Hartmann (2009) – Not to scale. At a certain radius from the star the disc is ionised into a plasma. This plasma can then be accreted onto the disc by following the strong magnetic field lines surrounding the star. **Page 2**
- 1.3:** **Figure 1.3:** The figure shows a planet undergoing Type I migration. The planet has a small mass so it is not able to open up a gap. This figure (and Figure 1.4, below) are taken from simulations done by Armitage & Rice (2005). The average surface density is given in the graph in the bottom left corner and shows that the surface density of the disc is greatest towards the centre and has lower values as radius increases. The planet can be identified as the yellow area above the centre. The wake of the planet can also be seen in the disc as a spiral, both internally and externally of the planet. **Page 6**
- 1.4:** An image from a simulation showing a planet undergoing Type II migration. A gap is clearly visible between the inner and outer regions of the disk with a region of high density around the planet. The surface density is plotted in the graph in the bottom left of the image. It shows the surface density dropping to around zero, at the inner edge of the gap, a small increase around the planet, a zero value on the other side of the planet before the surface density increases greatly at the outer edge of the disc. In the main image the density variations are very pronounced in the form of spirals, both internally and externally of the gap. **Page 7**
- 3.1:** A simulation image showing the logarithmic column density profile (in g cm^{-2}) of the initial conditions of a low mass disc ($M_{\text{disc}} = 0.005 M_{\odot}$, $R_{\text{disc}} = 15.2 \text{ AU}$) such as the one we used to test our code. High density regions are shown in red with very low density regions shown in blue. The edge of the disc is very clear and well defined. **Page 15**
- 3.2:** An example of a temperature profile created on a high mass disc with 1×10^6 particles. The temperature (given in Kelvin) follows an inverse square relationship as the main source of heat comes from the star. However, other considerations such as viscosity also play a part in the heating of the disc (as the disc evolves). **Page 16**
- 3.3:** SPH particle vertical positions against r for a low mass disc ($0.005 M_{\odot}$, left) and again for a high mass disc ($0.1 M_{\odot}$, right). The particles in the low mass disc have collapsed

less under their own gravity and therefore produce a much more flared disc profile compared to the high mass disc on the right **Page 17**

- 3.4:** The initial rotational velocity of SPH particles (in Kms^{-1}) for a 0.1 solar mass disc with 10^4 particles. The rotational velocity of the particles is exceptionally high at very low orbital radii but relatively low at greater distances from the star. **Page 18**
- 3.5:** Smoothing length (h) of the SPH particles in a high mass disc as a function of radius (given in AU). As the density of the disc increases with radius on the midplane, the smoothing lengths of the particles also increases. The diagram shows that particles very close to the star have small smoothing lengths which cover a narrow range of values, but particles at large radii from the star tend to have larger smoothing lengths in general and a much larger range of values. **Page 20**
- 4.1:** The plot above shows the initial logarithmic surface density (in units of g cm^{-2}) of the Ayliffe & Bate (2010) disc and the one on the right shows the surface density of the disc after the outer edge has completed three orbits. We then add a planet to the relaxed disc. This disc was evolved using the local isothermal model. The initial disc, as set up from our initial conditions (left) has an artificial looking very defined edge. In the image on the right, once the disc has evolved, the edges are more diffuse and the change in density is more gradual, as shown by the colour gradual change in colour. This represents a more natural disc. **Page 24**
- 4.2:** The images show the surface density of the disc after 25 yr, 625 yr 1500 yr and 2001 yr after the planet has been added. The column to the left shows the local isothermal model and that to the right shows the radiative transfer model. In this simulation the RT model does not include the radiative heating from the star. After 2001 yr the RT run shows the planet has opened up a more defined gap and had therefore removed more of the disc from its orbital path. The wakes of the planet are more refined in the RT models than in the local isothermal model. The local isothermal disc also becomes more extended over time. **Page 25**
- 4.3:** The planet orbital radius in the two runs with local isothermal shown in red and radiative transfer shown in green. The wobble which can be seen in each of the plots represents the eccentricity of the orbit. The rate of migration on the radiative transfer model is almost double that of the local isothermal model and therefore the total migration of the planet in the RT model is far greater. **Page 26**
- 4.4:** The semi-major axes of the planets in both the local isothermal and the radiative transfer methods. In the local isothermal run the migration of the planet is slower than in the radiative transfer run despite both following the same rate of inward migration for the first few orbits. From the gradients of the curves we can see that at 2000 years the rate of migration of the radiative transfer run is still greater than that of the local isothermal case. **Page 26**
- 4.5:** The eccentricity of the planets plotted against time for the two runs with the local isothermal model shown in red and the RT model shown in green. Despite following the same initial trend the local isothermal model shows generally less eccentricity than the

radiative transfer model. These very low values of eccentricity could be very well by noise from the smoothed hydrodynamics code itself. **Page 27**

- 4.6:** Accretion rates on the planets of the two test runs with local isothermal shown in red and the RT run shown in green. The general trend of accretion in each case is similar with the rate of accretion onto the planet in the local isothermal method being slightly higher overall. **Page 29**
- 5.1:** The initial surface density profiles of all four discs as a planet is added to them (units g cm^{-2}). The planets on the bottom row are of the $0.07 M_{\odot}$ disc and those on the top row are of the $0.1 M_{\odot}$ disc. The left two plots are of planets initially placed at 40 AU and the right two plots are of planets initially placed at 80 AU. **Page 31**
- 5.2:** The logarithmic surface density of the $0.1 M_{\odot}$ mass disc with the planet initially placed at 40 AU to the left and the planet initially placed at 80 AU on the right (in units g cm^{-2}). The density variations of the disc are apparent on the plots of the planet initially at 40 AU. Strong wakes can be seen with most prevalence at around 5000 yr. The gap opened by the planet at 80 AU is much wider than the gap opened by the planet at 40 AU. **Page 32**
- 5.3:** The semi-major axes of the two planets within the $0.1 M_{\odot}$ disc shows initial inward migration for both planets. The 80 AU planet (shown in green) has an initial rapid migration and then settles into a stable orbit. The 40 AU planet (shown in red) initially migrates inwards before starting migrating outwards throughout the rest of the run. **Page 34**
- 5.4:** Orbital radii of the two planets within a $0.1 M_{\odot}$ disc. The undulations in the radius indicate the eccentricity of the orbit and whilst these decrease for the 80 AU initial orbital radius planet (shown in green), the 40 AU initial orbital radius planet shows an increase in the eccentricity. **Page 33**
- 5.5:** The eccentricities of the two planets within the $0.1 M_{\odot}$ disc. The planet initially at 40 AU (shown in red) shows an eccentricity of 0.14 AU after 20 kyr. The decreasing and then almost constant eccentricity of the 80 AU initial orbital radius planet (shown in green) shows that it settles into a nearly circular orbit **Page 34**
- 5.6:** The masses (in M_{\odot}) of the two planets with the planet initially at 40 AU shown in red and the planet initially at 80 AU shown in green. Coincidentally both planets are the same mass after 20 kyr despite very different patterns of accretion. The pattern of the mass increase on the 40 AU planet indicates interactions with the disc as the bumps in the line indicate matter is added to the planet in bursts rather than a steady trickle. This is likely due to the areas of high and low density that the 40 AU initial radius planet passes through – see figure 5.8. **Page 34**
- 5.7:** The accretion rates onto planets in the two simulations. The initial peak (around 2.5 kyr) of the accretion rate onto the planet initially at 80 AU (shown in green) is caused by the rapid inward migration of the planet gaining access to fresh material as it moves through

the disc. The peaks seen in the planet initially at 40 AU are caused by interactions with the wakes of the planet moving through the disc shown in Figure 5.8 below. **Page 35**

- 5.8:** The inner region of the $0.1M_{\odot}$ disc with a planet originally placed at 40 AU. The wakes caused by the planet moving through the disc can clearly be seen (indicated by the arrow), including an area of high density which intercepts the orbit of the planet causing increased accretion and sudden bursts of new mass being added to the planet as shown by the bumps in the line on the graph in figure 5.6. **Page 35**
- 5.9:** Accretion onto the star in the $0.1 M_{\odot}$ disc with the planet initially at 40 AU shown in red and the planet initially at 80AU shown in green. The perturbations in the disc caused by the closer orbit of the 40 AU initial orbital radius planet cause more material to be accreted onto the star and the planet in closer proximity drives accretion as it forces matter inwards with its wake. The accretion onto the star in the disc of the planet initially at 80 AU continues to decrease throughout the course of the run. **Page 36**
- 5.10:** Logarithmic surface density profiles (in g cm^{-2}) of the runs with a $0.07 M_{\odot}$ disc. The two planets show different behaviours. The plots on the right are of the planet initially placed at 80 AU and show that the planet opens up a very large gap between 5 and 10 kyr. The final density of the rest of the disc is also far lower than that in the disc with the planet initially at 40 AU. Unlike the planet initially at 40 AU in the $0.1 M_{\odot}$ disc strong wakes have not formed in this disc due to its smaller mass. The 80 AU planet disc has a far less dense, more diffuse disc exterior to the planet compared with the 40 AU planet disc. **Page 37**
- 5.11:** The semi major axes of the two planets over the duration of the runs. The planet initially at 80 AU (shown above in green) has rapid initial inward migration as it clears the disc in its immediate vicinity. Migration then becomes outward but slower. The planet initially at 40 AU (shown in red) has a total inward migration of about 2-3 AU. **Page 38**
- 5.12:** A comparison of the orbital radii of both planets when placed into a $0.07 M_{\odot}$ disc. The 40 AU initial orbital radius planet (red) shows greater undulations on the graph above. Overall the migration of the 40 AU planet is very minimal with almost no overall migration from its original 40 AU radius. The initial inward migration of the planet initially at 80 AU (green) can also be seen for the first 2-3 kyr of the simulation. The undulations in both lines represent the eccentricity of the planets. **Page 38**
- 5.13:** The eccentricities of the two planets in the lower mass disc with the planet initially at 40 AU shown in red and the planet initially at 80 AU shown in red. The 40 AU planet's eccentricity becomes relatively high after being exceptionally low for the first half of the run. Despite this rapid rise these are still low values for eccentricity and represent an almost circular orbit. **Page 39**
- 5.14:** The increase in masses of the two planets over the course of the simulations. The increase in mass of the planet initially at 40 AU (shown above in red) is steady and has an almost constant gradient throughout. The 80 AU initial orbital radius planet has a rapid increase in mass between around 2,000-5,000 yr, before settling to a rate of mass increase very similar to that of the 40 AU initial orbital radius planet. **Page 40**

- 5.15:** : The logarithmic accretion rates of the planets within the lower mass disc with the planet initially at 40 AU shown in red and the planet initially at 80 AU shown in green. Both show artificially high rates of accretion at the very early stages of the simulation due to the planets being placed within a relaxed disc rather than being created within the disc. Over the first 3 – 4 kyr the 80 AU planet undergoes a very large accretion rate before steadily declining. The 40 AU planet has a much more erratic accretion pattern, especially over the last 5000 yr of the run. **Page 40**
- 5.16:** Accretion onto the star in the disc with a planet placed at 40 AU (shown about in red) is almost double that of the disc with a planet initially placed at 80 AU (shown above in green). As with the $0.1M_{\odot}$ discs the disc with the planet at a smaller orbital radius sustains a higher rate of accretion, likely due to the planet driving matter inwards towards the star. **Page 40**
- 5.17:** Surface density plots of the four simulations after 500 yr (with units g cm^{-2}). The plots on the left are the $0.1 M_{\odot}$ disc and on the right are the $0.07 M_{\odot}$. The top two plots are of the planets initially at 40 AU and the bottom two are for the planets initially at 80 AU. There are many similarities between the discs with the planets with similar initial orbital radii although the disc in the top left shows the most defined wakes of all four of the runs at this stage. **Page 41**
- 5.18:** The four simulations after 12,500 yr (surface density in units g cm^{-2}). The plots on the left are the $0.1 M_{\odot}$ disc and on the right are the $0.07 M_{\odot}$. The top two plots are of the planets initially at 40 AU and the bottom two are for the planets initially at 80 AU. Gaps are starting to form along the orbits of the planets. In the plots of planets initially at 40 AU the weak outline of spiral arms can be seen. **Page 42**
- 5.19:** The four simulations after 20,000 yr (surface density in units g cm^{-2}). The plots on the left are the $0.1 M_{\odot}$ disc and on the right are the $0.07 M_{\odot}$. The top two plots are of the planets initially at 40 AU and the bottom two are for the planets initially at 80 AU. Gaps are now fully formed and there is a significant difference between them. The higher mass disc plots show more structure within the disc and the lower mass discs show less pronounced dense regions. **Page 42**
- 5.20:** A comparison of all four planets' semi major axes over 20 kyr. All planets show initial inward migration, as they open up a gap, and all but the run3 planet show gradual outward migration over the remainder of the simulation. (Colours: Run1 → Red, Run2 → Green, Run3 → blue, Run4 → Purple). **Page 43**
- 5.21:** The eccentricities of all four planets over the course of the simulations. The two planets initially at 80 AU (shown here in blue and green) show the least change in eccentricity with the Run1 planet (shown in red) showing the greatest increase in orbital eccentricity. Despite this seemingly large increases, these values are very low and represent a near circular orbit. **Page 44**
- 5.22:** The mass of all 4 planets increases markedly throughout the simulation. The two planets initially at 80AU show a similar pattern to their mass increase, with the greatest rate of

change being during their migration phase. All planets except that in Run1 have a similar mass-gradient from around 10 kyr, indicating that the accretion rates of gas onto them are similar. The Run1 planet is likely different due to it having the greatest interaction with the spiral arms in the more massive of the two discs. **Page 45**

5.23: The mass of the disc and the initial radius of the planet has a very marked difference on the accretion rates of the planets. Despite all having peaks within 5,000 yr, due to their initial migration and gap opening, the accretion patterns of the planets are very different. **Page 46**

5.24: The accretion rate onto the star for all four simulations. The rates of accretion for the star in the lower mass disc (shown in purple and blue) are less than those in the higher mass disc (shown in red and green). This is simply due to less material being available for accretion in the lower mass disc. In both of the discs with the smaller orbital radius planet, accretion onto the star is greater than in the discs with a more distant planet and the planet cannot drive accretion from such distances. **Page 46**

List of Tables

- 4.1:** Table 4.1 shows the semi major axis (α), migration time scale (τ) and mass of the two planets in each of the runs at or between specific times in each simulation. By taking two values of α , the migration timescale can be calculated between those two points. The larger the migration timescale the slower the migration of the planet. We do not take very early values of migration timescale into account here as the planet has been placed in the disc rather than organically forming there which means that the opening of a gap for planet will produce and unnaturally rapid migration.. **Page 28**
- 4.2:** Migration timescales of both simulations presented in this chapter and the values obtained in AB2010. The values we obtain are comparable with the ones from AB2010, which suggests that our code is reliable. Our radiative transfer values are likely different to those in AB2010 due to the increase in planet mass over the course of the run. In the AB2010 RT run the planet mass remained fixed at the initial mass which causes a change in migration timescale overall. **Page 29**
- 5.1:** The initial parameters of all four runs and how they will be referred to from this point onwards. **Page 31**
- 5.2:** The semi-major axis, α , of the planets in the four different runs at set time intervals throughout the 20 kyr evolution of the disc. The Run1 planet shows an overall trend towards outward migration with the semi major axis of this planet being greater at the end of the simulation that it was at the start of the run. All other runs show overall inward migration. However, both Run2 and Run4 show slight outward migration after 6000 yr. **Page 43**
- 5.3:** The final masses of the four planets it is purely coincidental that the two planets in run1 and run2 have such similar final mass values. In figure 5.22 these two runs appear to end at the same value however using the data directly it can be seen that there is a difference of around $1M_j$ (to two significant figures) between them.. **Page 45**
- 5.4:** The migration timescales at the times listed in Table 5.3 of the four planets show that the migration is mostly outwards after an initial burst of inward migration. Inward migration is shown in green and outward migration is shown in red. These are the migration timescales of each of the planets taken at the same four times after the initial 2000 yr of the run. This is done so the planet and disc are settled into their orbit and the sudden, very high accretion rates caused by the planet being placed into a fully formed disc aren't taken into account **Page 47**

5.5: The rates of migration at the times listed in Table 5.3 for each of the runs shows both inward (shown in green) and outward (shown in red) migration throughout the simulation. These rates of migration are calculated by dividing the change in semi-major axis between two times by the amount of time that has passed. Each of the migration rates in the table above are averages taken over 1000 yr timeframe. The minus sign simply indicates the direction of migration is not inwards. Initially Run2 shows the highest rate of migration, moving inwards at a rate of 0.01 AU per year **Page 47**

Chapter 1

Introduction

1.1 The Formation of a Disc

Before a planet forming, protoplanetary disc can be formed, an initial molecular cloud must first be present. These molecular clouds are cool in temperature allowing for presence of molecules, rather than ionised gases which are present in higher temperature clouds. Protoplanetary discs are primarily made up of molecular gas (mostly molecular hydrogen) with heavier elements also present in the disc. From the planets present in our Solar system the minimum mass of the nebula which is required to produce these planets can be derived. This is known as the Minimum Solar Mass Nebula and is approximately $0.01 M_{\odot}$.

The disc is formed quickly after the collapse of the initial molecular cloud. This collapse could happen due to shock waves from other events such as a relatively near-by supernova. The disc shape forms due to the angular momentum of its parent cloud.

The parent molecular cloud has a very low rotational velocity but its angular momentum is large ($\sim 10^{54} \text{ g cm}^2 \text{ s}^{-1}$; Armitage 2007). This value of angular momentum is far greater than the angular momentum of the solar system. This problem is referred to as “the angular momentum problem” of star formation (Armitage 2007).

Protostellar discs have masses of a few percent of M_{\odot} (up to $0.1\text{-}0.2 M_{\odot}$ in some cases) and typical radii of $\sim 100 \text{ AU}$. Most discs are flared (Figure 1.1a), i.e. they get thicker as the radius increases. The higher the mass of the disc, the more its own gravity will cause it to flatten, giving it a less flared appearance (Figure 1.1b).

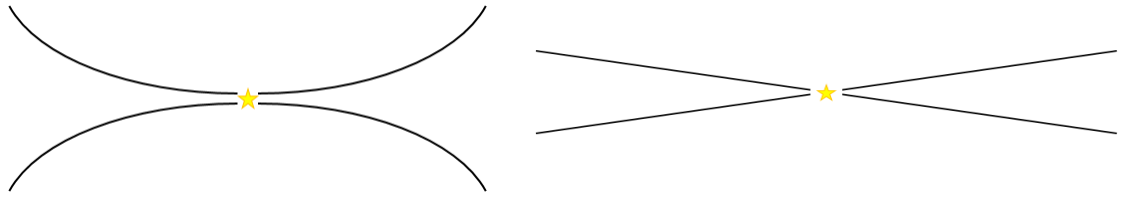


Figure 1.1: (a) Left: An example of a low mass, flared disc as seen edge-on. (b) Right: An example of a less flared, more massive disc. As the mass of the disc is proportional to the mass of the star at its centre, a more massive disc with a more massive star will not only have the increased self-gravity giving it a less flared profile but also will have a greater vertical component of the star's gravity pulling it towards the mid-plane.

The conditions that exist in the region of the disc closest to the central star are rather extreme. The high temperatures turn the gas into a charged plasma. A gap will be opened up between the disc and the star due to the stellar magnetic field and gas will accrete onto the star along the magnetic field lines towards the north and south poles (Figure 1.2). This gap is then increased further when the intense UV radiation from the star causes photoevaporation of the disc from the inside outwards. There can still be accretion across this gap however, rather than being continuous, it is likely that gas will cross this gap in bursts.

The problem with this form of accretion is that it does not account for the loss in angular momentum caused by the disc material falling onto the star and the star does not rotate as quickly as it should in order to account for this gain in angular momentum. The solution to this is likely jets at the poles of the star spiralling some of the material outwards into space and thereby conserving angular momentum.

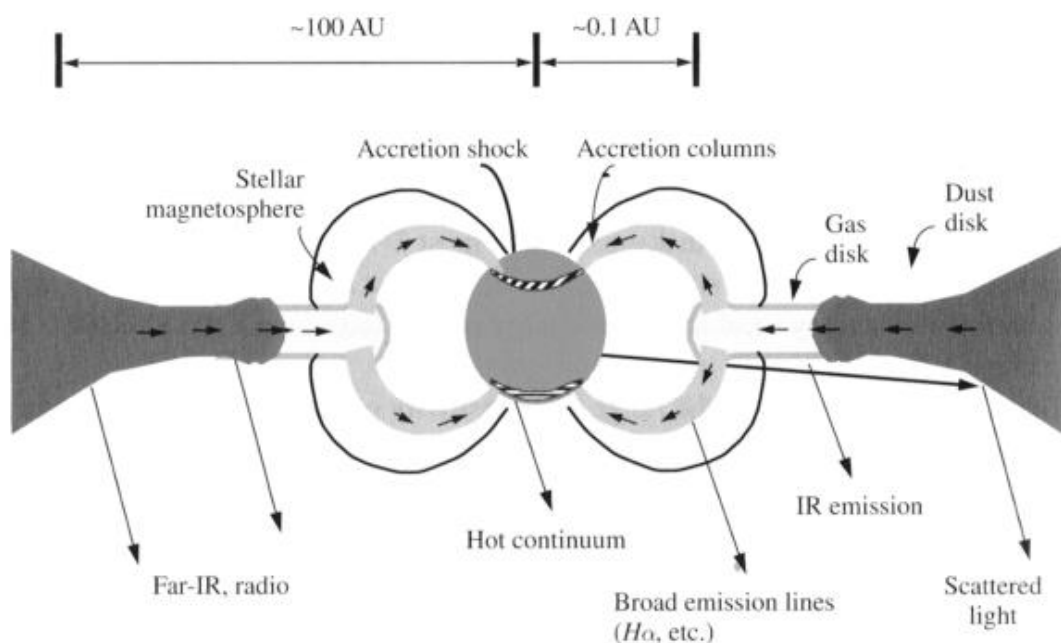


Figure 1.2: A diagram showing how accretion occurs due to accretion columns close to the star, Hartmann (2009) – Not to scale. At a certain radius from the star the disc is ionised into a plasma. This plasma can then be accreted onto the disc by following the strong magnetic field lines surrounding the star.

1.2 The Formation of Planets

There are currently two main scenarios which may explain the formation of planets within a protoplanetary disc: the core accretion model and the gravitational fragmentation model. Core accretion is the likely method for the formation of lower mass, rocky planets and gravitational fragmentation could be the method responsible for the creation of massive planets which form at distances of greater than around 20 AU from the central star (Boss 2011).

1.2.1 The Core Accretion Model

In the core accretion model dust particles collide and stick together within the disc, gradually getting larger. Not all collisions produce a growth however, as, if their relative velocities are too great, the particles will fragment into smaller grains rather than stick together to form a larger particle; in fact, very few bodies are able to grow past a metre in size (Garaud et al. 2013). The presence of water ice acts as a sort of glue which “sticks” the dust together, therefore this process is more efficient at radii far enough away from the star that the intense stellar radiation does not sublimate the ice away. From this process dust grows from sub-micron size to planetesimals (km-sized objects). Larger planetesimals are able to sweep up more dust from the disc and a few of them dominate. It has been suggested by Pollack et al. (1996) that this is the first of three stages required to build a stable planet and this part of the process takes planet with a timescale in the region of 0.5 Myr.

Once this initial phase has been completed the planet has removed material from its orbit and, therefore, can only, very slowly, accrete more mass from the surrounding disc. During this time the planet is in a precarious hydrostatic equilibrium (Phase II).

Once a planetesimal reaches a critical mass ($\sim 10 M_{\text{Earth}}$) it is able to accrete a gaseous envelope rapidly (Phase III). This sudden increase in mass gives the planet a larger potential well causing more material to accrete on to the planet and eventually causes a runaway phase in which rapid planet growth takes place.

The final phase of core accretion usually occurs within 7.5 Myr, when the mass of the core and the mass of the surrounding gaseous envelope is approximately equal in mass and hydrostatic equilibrium has once again been reached.

1.2.2 Gravitational Fragmentation

At radii greater than around 30 AU there is not enough material present to form a several Jupiter mass planet if building a planet by colliding dust particles together to form larger and larger bodies. According to the disc fragmentation theory a massive disc can become gravitationally unstable and fragment to form gas giant planets at large distances from the central star.

This method requires the disc to be massive enough to be gravitationally unstable and to be able to cool fast enough. The first condition is described by the Toomre criterion (Toomre 1964):

$$Q = \frac{c_s k}{\pi G \Sigma} < 1 \quad (1.1)$$

where Q is the Toomre parameter, c_s is the local speed of sound, k is the epicyclic frequency (which is equal to the rotational velocity for Keplerian discs), G is the gravitational constant and Σ is the surface density of the disc. For the second condition to be fulfilled the disc needs to be able to cool on a dynamical timescale, i.e. within a few orbital periods. Numerical studies (e.g. Gammie 2001; Rice et al. 2003) suggest that the cooling rate needs to be:

$$t_{cool} \sim (0.5 - 2) t_{orb} \quad (1.2)$$

The most frequent outcome of disc fragmentations are brown dwarfs but planets may also form (Stamatellos & Whitworth 2009). A planet becomes a brown dwarf at masses above $13 M_J$. At this point the mass is great enough that the pressure and temperature within the core will allow deuterium fusion to take place. Observations suggest that only 10% of giant planets may form by this method however, with the remaining being formed by core accretion (Matsuo et al. 2007). The mass of the central protostar also has an effect on the formation of a planet via gravitational fragmentation. This is likely because the mass of the star is proportional to the mass of the disc. Therefore, a larger star will have a larger disc and the fragments produced may be more massive than planets or even brown dwarfs.

Originally it was presumed that most planets would form via core accretion. However, our understanding of the process suggested that the timeframes required for the larger planets to form was greater than the observed lifespans of protostellar discs; giant planets are forming far more quickly than the original core accretion method would allow. Observations have shown that many giant planets have been found in the regions of the disc which are cool enough for

ice to be present. As the timescale of planet formation is dependent on the amount of material available to create the planet, it follows that giant planets would form most quickly in this region (Armitage 2007). Planets with masses of several Jupiters were also discovered close to their host star at distances <1 AU (51 Peg b is the first hot Jupiter to be discovered; it has an orbital period of 4.2 days; Mayor & Queloz 1995). Such planets could not have been formed in these locations due to the lack of material available at such small orbital radii. The conditions at these radii would also make the formation of such massive planets impossible due to the very large temperatures associated with close proximity to a star. At a thousand Kelvin the dust particles themselves would sublimate. Observations have shown that hot Jupiters tend to be the lone planet in orbit of a star whereas stars which do not have a giant planet in very close proximity to the star will usually have multiple giants in their planetary system (Hartman et al. 2014).

1.3 The Migration of Planets

Core accretion had initially not taken into account the migration of planets within the disc. This inward movement of a planet during its formation may remove a few of the barriers which the model had come up against when dealing with objects of mass in the order of several Jupiters. If a planet formed at large distances from its star and then migrated inwards, it would have a constantly replenished supply of disc material which to accrete as it moved towards the central star (Lin et al. 1996).

1.3.1 Type I Migration

Smaller-mass planets within a system undergo Type I migration due to interactions within the protoplanetary disc. Type I migration occurs for planet masses of around 0.1 of Jupiter's mass (Bate et al. 2003). During type I migration the low mass planet remains embedded within the disc and does not open up a gap. Torques develop at the inner and outer edges of the planet's orbit as it moves through the viscous disc. The rate of migration is dependent on the difference between the inner and outer torque. If the difference is in the region of 0 then the planet will remain at a constant radius from the star as the planet would act as a source of angular momentum transport within the disc (Goodman & Rafikov 2001). In the case of a small-mass planet the torque results in inward migration (Type I). Type I migration is at its most rapid at the

point which a smaller-mass planet gains enough mass, through accretion, to start to open up a gap on its orbit. As this gap first starts to form (Figure 1.3) Type I migration is at its peak. Eventually this gap will be fully open and Type I migration will stop.

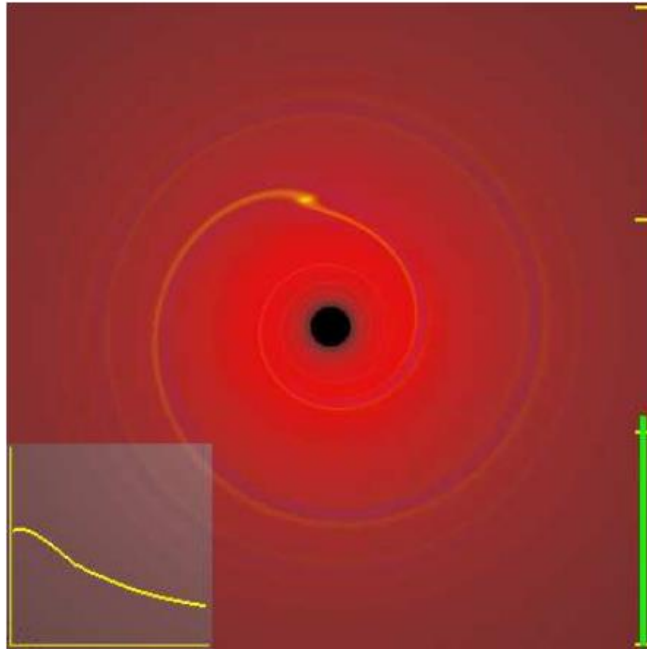


Figure 1.3: The figure shows a planet undergoing Type I migration. The planet has a small mass so it is not able to open up a gap. This figure (and Figure 1.4, below) are taken from simulations done by Armitage & Rice (2005). The average surface density is given in the graph in the bottom left corner and shows that the surface density of the disc is greatest towards the centre and has lower values as radius increases. The planet can be identified as the yellow area above the centre. The wake of the planet can also be seen in the disc as a spiral, both internally and externally of the planet.

1.3.2 Type II Migration

The Hill Sphere of a planet is given by:

$$\left(\frac{GM_*}{\alpha^3}\right)^{\frac{1}{2}} = \left(\frac{GM_p}{r_h^3}\right)^{\frac{1}{2}} \quad (1.3)$$

Where M_* is the mass of the star, M_p is the mass of the planet, α is the semi major axis and r_h is the Hill radius. This radius defines the planet (or star's) gravitational sphere of influence. Larger-mass planets (with a Hill sphere radius in the same order as the disc thickness) tend to undergo Type II migration. As their Hill radius is around the same size as the thickness of the disc, they will rapidly accrete all material reaching out to the upper and lower edges of the disc. As a planet forms it carves out a gap within the disc as it adds that material to its own mass

(Figure 1.4). In order for a gap to be produced the tidal torque must remove material from the gap faster than the disc viscosity and thermal pressure can fill it back in again (Goldreich & Termaine 1980). The exchange of angular momentum in the disc due to viscous forces moves the gas in the disc and the gap within it, along with the planet that created it, inwards. The efficiency of the angular momentum transfer within the disc is the factor that determines the rate of migration of a planet in the Type II regime. This type of migration is much slower than Type I migration.

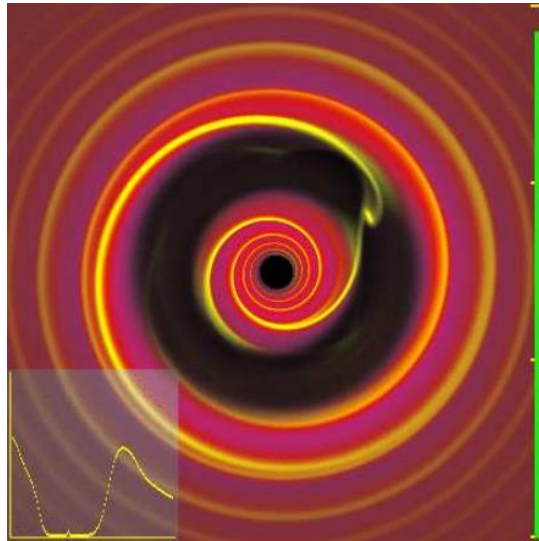


Figure 1.4: An image from a simulation showing a planet undergoing Type II migration. A gap is clearly visible between the inner and outer regions of the disk with a region of high density around the planet. The surface density is plotted in the graph in the bottom left of the image. It shows the surface density dropping to around zero, at the inner edge of the gap, a small increase around the planet, a zero value on the other side of the planet before the surface density increases greatly at the outer edge of the disc. In the main image the density variations are very pronounced in the form of spirals, both internally and externally of the gap.

Type II migration allows for planets with several Jupiter masses to exist at small distance from the host star.

Type I and Type II migration can only occur if a disc is present. Migration will therefore stop once the disc has dispersed. Theoretically the disc should slowly be evaporated, accreted or otherwise dispersed gradually over a large time frame.

There are other types of migration which can occur once the disc itself has dissipated due to interactions between planets in a multi-planet system or collisions between planets before they have settled in to stable orbits. This migration can be both inwards and outwards and in some cases can eject a planet from a system. It is likely that the current position of Neptune was caused by such migration (Gomes et al. 2005).

1.4 Thesis outline

The goal of this thesis is to study the migration of giant planets that are initially on wide orbits (~ 50 AU) in newly formed protostellar discs. Such planets may have formed by disc fragmentation very early after the formation of the disc. At this early phase, protostellar discs may be relatively massive ($\sim 0.1-0.3 M_{\odot}$) and, therefore, close to being gravitationally unstable (e.g. Stamatellos et al. 2011)

In Chapter 2, we describe the background of the computational method that we use for the simulations (Smoothed Particle Hydrodynamics).

In Chapter 3, we discuss in detail how the initial conditions of the discs that we use for our simulations are constructed.

In Chapter 4 we test the code and compare our findings to those of previous studies (Ayliffe & Bate 2010; hereafter AB2010). We compare the migration timescales of giant planets in low-mass discs with the ones found by AB2010 for locally isothermal discs and for discs where the radiative transfer is taken into account.

In Chapter 5, we simulate the evolution of giant planets that are initially on wide orbits in massive protostellar discs. We examine how planet migration is affected by the initial orbital radius of the planet and by the mass of the protostellar disc.

Finally, in Chapter 6 we summarize our conclusions.

Chapter 2

Smoothed Particle Hydrodynamics

2.1 Introduction

Smoothed Particle Hydrodynamics (SPH; see reviews by Monaghan 1992, 2012) is a way of modelling the dynamics of a fluid by viewing it as an ensemble of particles. The larger the number of particles that are used the better the representation of the fluid. Each of the particles representing the fluid experience forces due to viscosity, pressure and gravity, from the other particles within the system.

The two main ideas of SPH have been summarised by Martin et al. (1993) as:

1. The properties of the fluid at any point are estimated by taking a weighted average of those properties over the surrounding volume.
2. The continuum is approximated by a finite number of particles which are free to move under their mutual interaction and the action of any external body forces.

SPH solves the following equations for a gaseous, viscous disc:

Continuity Equation:

$$\frac{\delta\rho}{\delta t} + v \cdot \nabla\rho = -\rho\nabla \cdot v \quad (2.1)$$

Momentum Equation:

$$\frac{\delta v}{\delta t} + v \cdot \nabla v = -\frac{\nabla P}{\rho} - \nabla\phi + F_{viscous} \quad (2.2)$$

Energy Equation:

$$\frac{\delta u}{\delta t} + v \cdot \nabla u = -\frac{P}{\rho} \nabla \cdot v + \frac{\Gamma - \Lambda}{\rho} \quad (2.3)$$

where ρ is density of the fluid, v is the velocity, P is the pressure, ϕ is the gravitational potential, $F_{viscous}$ is the viscous force per unit mass, u is the thermal energy per unit mass, Γ is the heating function and Λ is the cooling function of the fluid.

An equation of state is also required to close the equations. This is based on the degree of dissociation and ionisation of hydrogen and helium within the simulation as in Stamatellos et. al (2007). For densities up to approximately 0.03g cm^{-3} , the ideal gas approximation will hold true and is given by:

$$P_i = \frac{\rho_i k_B T_i}{\mu_i m_H} \quad (2.4)$$

2.2 Smoothing Kernels

In SPH a smoothing kernel is used which gives a weighted mean of a specific property over a local volume of a set radius. The radius of this kernel, or smoothing length, h , is varied so that the same number of particles in a sphere of radius $2h$ around each particle is used to calculate the weighted mean. The smoothing volume, V , is therefore

$$V = \frac{Nm_j}{\bar{\rho}} = \frac{4}{3}\pi(2h)^3 \quad (2.5)$$

In a densely packed region of a disc, for example close to the central star, the value of h will be small, whereas at several hundred AU the smoothing length will be much greater as to include the same number of particles within $2h$. The varying value of h allows the model to have high resolution in areas where it is required, optimising the use of computing power.

The most commonly used kernel is the Beta-Spline kernel (Monaghan & Lattanzio 1985):

$$W(r, h) = \frac{\pi}{h^3} \begin{cases} 4 - 6x^2 + 3x^3 & 0 \leq x < 1 \\ (2 - x)^3 & 1 \leq x < 2 \\ 0 & x \geq 2 \end{cases} \quad (2.6)$$

where $x=r/h$.

2.3 Time Steps

SPH calculations need to have an appropriate time step in order to achieve an accurate simulation. There are a series of conditions which must be satisfied in order to calculate an appropriate time step for the simulation. Each particle has a maximum time step as given by the equation:

$$\Delta t_{max}^i = \gamma \min(\Delta t_v^i, \Delta t_{\sqrt{v}}^i, \Delta t_a^i, \Delta t_{cv}^i), \quad (2.7)$$

where $\gamma \sim 0.2 - 0.3$ is a proportionality constant.

The four terms in the above relation are responsible for ensuring that the length of a time step is never great enough to allow changes in particle positions to be greater than smoothing length, h , the changes in relative velocity and local density are small for any given time step, and that viscous forces do not change by much between successive time steps. Ideally the time step for any given simulation would be the smallest assigned time step for any of the particles within the disc. In real terms this is impractical due to the time each simulation would take to run, therefore a minimum time step is defined, as are several larger multiple time steps that are appropriate for different particles.

2.4 The Barnes-Hut Tree

As each particle has a mass, it has gravitational influence over all the other particles within the system. If every particle were treated as an individual particle in relation to all other particles, irrespective of distance, then the simulation would take an exceptionally long time to complete, as gravitational forces will need to be computed from all particles individually. A way to get around this problem is to use a recursive spatial tessellation octal tree as developed by Barnes and Hut (1986). Other types of trees can be used in SPH but the Barnes – Hut tree is used in the SEREN code, which will be used for this project.

All of the particles within the disc are contained within a virtual root cell, which is then split into eight subcells of equal size. These cells are then subdivided once more until each subcell contains no more than one particle. The gravitational forces acting on each of the particles are calculated by measuring its distance from the centre of each cell. If the particle is close to the centre of a cell then that cell is opened into subcells. If a particle is a large distance away from the centre of a cell then the whole cell is taken to act as a single source of gravity, rather than the individual particles within the subcell. The single source is assumed to act from the centre of mass of the cell. It is in this way that subcells closest to a particle are opened and their individual gravitational influences are calculated for that particle and ones at greater distances are calculated en mass, with larger cells, and more particles being combined at greater distances from the particle in question.

The other forces acting upon a particle, such as viscosity and pressure are only applied to any particle by the particles directly around it (within a distance of $2h$). A second run is required to find the *neighbours* of each particle. In this tree, a series of cubes are created centred on a given particle. If the cells overlap, then they are opened into subcells and again if an overlap is found further sub cells are opened. This process is continued until the given particle is at the centre of the final cube and its *neighbours* have been found.

2.5 Sink Particles

In simulations in which high densities are attained (e.g. when stars or planets are forming), when the density exceeds a pre-defined value ($\sim 10^{-9} \text{ g cm}^{-3}$) a gas particle is replaced by a sink particle which interacts only gravitationally with its environment. This is to avoid exceptionally small time steps that would make the simulation computationally time consuming. Gas SPH particles

can be accreted onto a sink increasing its mass, if they are within the sink radius ($\sim 1\text{AU}$) and are gravitationally bound to the sink (e.g. Bate et al. 1996).

2.6 SEREN SPH Code

We will model protostellar discs using the Smoothed Particle Hydrodynamics code SEREN (Hubber et al. 2011). The code uses an octal tree similar to the Barnes-Hut Tree (Chapter 2.4), multiple timesteps (Chapter 2.3), and a 2nd-order Runge-Kutta integration scheme. The code uses time-dependent artificial viscosity with parameters of shear viscosity; $\alpha_{\min} = 0.1$ and $\alpha_{\max} = 1$ and β (which stops a particle from passing through another particle) = 2α , which reduce time dependent viscosity in shock regions and artificial shear viscosity (Morris & Monaghan 1997).

The chemical and radiative processes that regulate the gas temperature are treated with the approximation of Stamatellos et al. (2007). This approximation gives each SPH particle a pseudo cloud which allows the particle to heat and cool through a radiative transfer method. The method takes into account compressional heating, viscous heating, radiative heating by the background, and radiative cooling as laid out in Stamatellos, Hubber & Whitworth (2007). We can calculate this using:

$$\left. \frac{du_i}{dt} \right|_{RAD} = \frac{4\sigma_{SB}(T_{BGR}^4 - T_i^4)}{\Sigma_i^2 \bar{K}_R(\rho_i, T_i) + K_P^{-1}(\rho_i, T_i)} \quad (2.8)$$

This equation ensures that the temperature of the SPH particle never drops below the background temperature, T_{BGR} . $K_P^{-1}(\rho_i, T_i)$ is the Planck-mean opacity, and σ_{SB} is the Stefan-Boltzmann constant. We use opacity tables which are appropriate for protostellar discs (Bell & Lin 1994).

Chapter 3

Setting up the Disc Initial Conditions

3.1 Introduction

In order to run simulations using the SEREN code (Hubber et al. 2011) initial conditions need to be laid out for the disc. Here, we deal with the migration of giant planets and therefore use a sink particle placed within the disc to represent the planet as part of the initial conditions rather than allowing a planet to form self-consistently, e.g. by disc fragmentation (Stamatellos 2013).

3.2 Disc surface density and mass

In order to study the migration process of massive planets, a disc must first be set up. The surface density of the disc is given by

$$\Sigma(R) = \Sigma_0 \left(\frac{R_0^2}{R_0^2 + R^2} \right)^{\frac{p}{2}} \quad (3.1)$$

where Σ_0 is the surface density when the radius is 0, R_0 is a softening radius which is used to stop the density of the disc becoming unrealistically large close to the surface of the star and R is the mid plane distance from the star to the particle. p indicates how quickly the density drops with radius and is given a value of 1.

Figure 3.1 below shows these initial surface density conditions using 2×10^5 particles. These conditions were used to test the code.

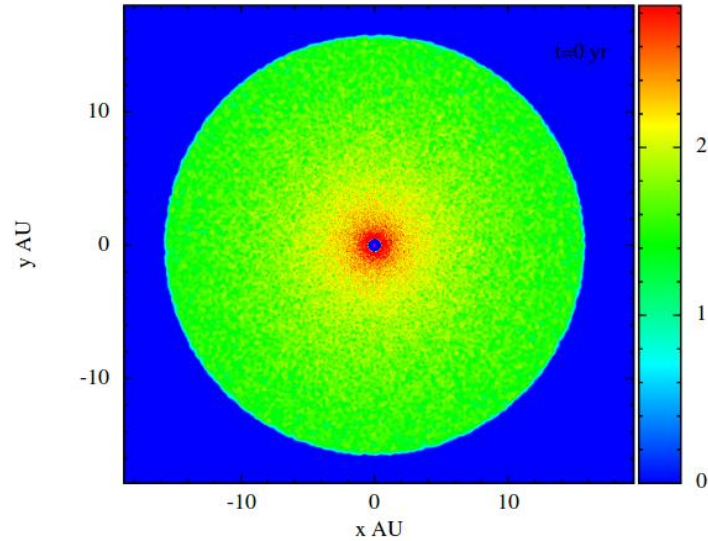


Figure 3.1: A simulation image showing the logarithmic column density profile (in g cm^{-2}) of the initial conditions of a low mass disc ($M_{\text{disc}} = 0.005 M_{\odot}$, $R_{\text{disc}} = 15.2 \text{ AU}$) such as the one we used to test our code. High density regions are shown in red with very low density regions shown in blue. The edge of the disc is very clear and well defined.

Set in the $x - y$ plane the mid-plane distance can be found by

$$R = \sqrt{x^2 + y^2} \quad (3.2)$$

By integrating the surface density and substituting for $\Sigma(R)$ the mass of the disc interior to that radius can be found. If the radius of the disc is used (R_{disc}) then the mass of the entire disc can be calculated using

$$M_{\text{disc}} = \pi R_0^2 \Sigma_0 \left[\left(\frac{R_0^2 + R_{\text{disc}}^2}{R_0^2} \right)^{1-\frac{p}{2}} - 1 \right] \quad (3.3)$$

As the total mass of the disc is an input parameter in solar masses, this equation can then be rearranged to find a value for Σ_0 :

$$\Sigma_0 = \frac{M_{\text{disc}}}{R_0^2 \pi} \left[\left(\frac{R_0^2 + R_{\text{disc}}^2}{R_0^2} \right)^{1-\frac{p}{2}} - 1 \right]^{-1} \quad (3.4)$$

p is set to a value of 1 as established from observations.

3.3 Disc Temperature Profile

The temperature profile of a passive disc depends on the mass of the star M_\star , the temperature of the star T_\star , the radius of the star R_\star and the luminosity of the star L_\star . We parameterise the disc temperature profile as follows

$$T_d(R) = \left[T_0^2 \left(\frac{R^2 + R_0^2}{AU^2} \right)^{-q} + T_\infty^2 \right]^{1/2} \quad (3.5)$$

This is an assumption based upon theory and observational data. In the above Equation, T_0 is the temperature at a radius of 1AU and R_0 is the softening radius which stops the temperature of the disc becoming unnaturally high at small distances from the star. T_∞ is the background temperature set to 10 K. The value of q is set at 0.5; therefore, the temperature profiles of the discs we create will all be similar. The value of q is set at 0.5 as our disc is flared. If a flat disc were flat $T \sim r^{-3/4}$ would be the appropriate approximation.

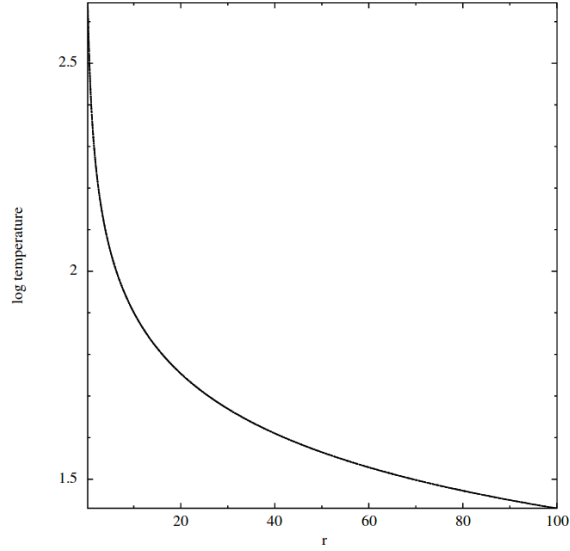


Figure 3.2: An example of a temperature profile created on a high mass disc with 1×10^6 particles. The temperature (given in Kelvin) follows an inverse square relationship as the main source of heat comes from the star. However, other considerations such as viscosity also play a part in the heating of the disc (as the disc evolves).

3.4 Disc vertical density profile and disc thickness

By balancing the forces it can be shown that the thickness of the disc (z_0) at a radius (R) is given by:

$$z_0(R) = -\frac{\pi \Sigma(R) R^3}{2M_\star} + \left[\left(\frac{\pi \Sigma(R) R^3}{2M_\star} \right)^2 + \frac{R^3}{GM_\star} c_s^2(R) \right]^{1/2} \quad (3.6)$$

where $c_s(R)$ is the local speed of sound and is found by

$$c_s(R) = \sqrt{\frac{kT(R)}{\mu m_H}} \quad (3.7)$$

M_\star is the mass of the central star, G the gravitational constant, k is the Boltzmann constant, μ is the mean molecular weight (2.3) and m_H is the mass of the hydrogen atom. Discs are rather flat but they do have a thickness (usually this is around 10% of the disc radius). A lower mass disc (with mass in the order of 0.01 of the central star) will more flared, while a larger mass disc (in the order of 0.1 of the central star) will be flatter and less flared. This comparison can be seen in Figure 3.3 below. The thickness profile is found by balancing the force of the disc pushing vertically outwards, caused by thermal pressure, and force of gravity from the star pulling the disc vertically inwards. In reality a large mass disc of around $0.1 M_\odot$ would also experience a significant vertically inward force caused by the weight of the disc itself. This further flattens the disc.

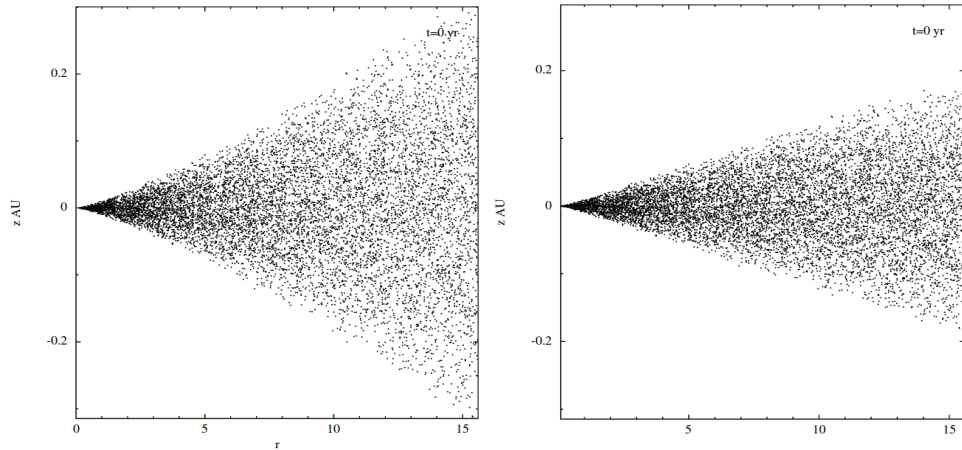


Figure 3.3: SPH particle vertical positions against r for a low mass disc ($0.005 M_\odot$, left) and again for a high mass disc ($0.1 M_\odot$, right). The particles in the low mass disc have collapsed less under their own gravity and therefore produce a much more flared disc profile compared to the high mass disc on the right.

We set the volume density of the disc to decrease with distance from the mid-plane following a cosine profile given by

$$\rho(R, z) = \frac{\pi \Sigma_0}{4z_0(R)} \left(\frac{R_0^2}{R_0^2 + R^2} \right)^{p/2} \cos \left[\frac{\pi z}{2z_0(R)} \right] \quad (3.8)$$

This is similar to a Gaussian profile but with a value equal to zero at a finite distance. The rotation of the disc is considered to be independent of the vertical distance from the midplane. We consider that there is no initial motion in the z direction and therefore the initial vertical velocities will all be equal to 0. Figure 3.3 charts the difference between two similar discs, each with 10^4 particles, a disc radius of 15.2AU and a central gap of 0.1 AU. The mass of the central star is set to $1 M_\odot$. The only difference is the mass of these two discs: the one on the left has 20 times the mass of the one on the right.

3.5 Disc velocity profile

The velocity of the disc is set to be Keplerian, therefore for a particle i ,

$$v_i = \left(\frac{[GM_\star + M(R_i)]}{R_i} \right)^{1/2}, \quad (3.9)$$

with the velocity of each SPH particle (assuming anti-clockwise rotation) found from

$$v_{x,i} = -v_i \frac{y_i}{R_i} \quad (3.10)$$

$$v_{y,i} = +v_i \frac{x_i}{R_i} \quad (3.11)$$

Therefore, the velocity of each particle in the $x - y$ plane can be found simply using

$$v_i = \sqrt{v_{x,i}^2 + v_{y,i}^2} \quad (3.12)$$

A more massive disc has a higher velocity (for a given radius) due to acceleration caused by the disc's self-gravity whereas a lower mass disc will be mostly influenced by the acceleration due to the gravity of the star. Figure 3.4, below, shows the initial velocity profile of a large mass disc with a radius of 100AU.

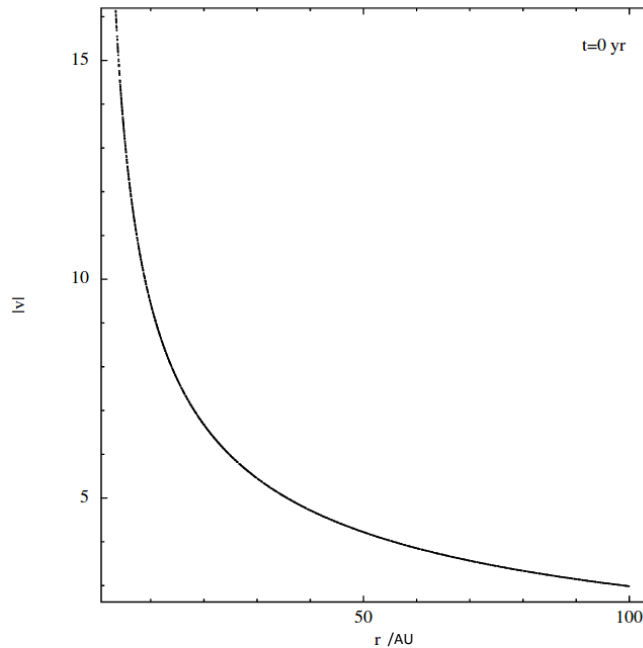


Figure 3.4: The initial rotational velocity of SPH particles (in Kms^{-1}) for a 0.1 solar mass disc with 10^4 particles. The rotational velocity of the particles is exceptionally high at very low orbital radii but relatively low at greater distances from the star.

3.6 Setting up the positions and masses of the SPH particles

In an SPH simulation particles are distributed using random numbers ($\mathcal{R}_1\mathcal{R}_2\mathcal{R}_3$) to generate the required density profiles given by eq. (1) and (8)

To calculate the distance R of a particle on the disc midplane we assume

$$\frac{M(R)}{M_{disc}} = \mathcal{R}_1 \quad (3.13)$$

The radius of each particle is set to

$$R = R_0\omega^{1/2} \quad (3.14)$$

From equations (3.13), (3.14) and (3.3) we find:

$$\omega = \{(1 + \omega_{in})^{1-(p/2)} + \mathcal{R}_1[(1 + \omega_{out})^{1-(p/2)} - (1 + \omega_{in})^{1-(p/2)}]\}^{2/(2-p)} - 1 \quad (3.15)$$

As this disc will have inner and outer boundaries, we assume

$$\omega_{in} = \frac{R_{in}^2}{R_0^2} \quad (3.16)$$

and

$$\omega_{out} = \frac{R_{out}^2}{R_0^2} \quad (3.17)$$

where R_{in} is the inner radius of the disc and R_{out} is the outer boundary of the disc. Thus, we set the azimuthal angle ϕ using a random number \mathcal{R}_2 ,

$$\phi = 2\pi\mathcal{R}_2 \quad (3.18)$$

the x and y coordinates are

$$x = R \cos(2\pi \mathcal{R}_2) \quad (3.19)$$

$$y = R \sin(2\pi \mathcal{R}_2). \quad (3.20)$$

To calculate the z-coordinate we set

$$\frac{\Sigma(R, z)}{\Sigma(R, z_0)} = \mathcal{R}_3. \quad (3.21)$$

The z coordinate of the particle is found from:

$$z = z_0(R) \frac{2}{\pi} \sin^{-1}(2\mathcal{R}_3 - 1) \quad (3.22)$$

The mass of an SPH particle (m_i) is found by dividing the mass of the disc by the number of particles present in the disc for each simulation.

3.7 Setting up the smoothing length of the SPH particles

The smoothing length of the particles (h_i) is found as each particle must have $N_{\text{neigh}}=50 \pm 5$ neighbouring particles (N_{neigh}) within a sphere of radius $2h$ centred on the particle in question.

Therefore, the smoothing length is found using:

$$h_i = \left[\frac{3N_{\text{neigh}}m_i}{32\pi\rho(R_i, z_i)} \right]^{1/3} \quad (3.23)$$

Figure 3.5 below shows the smoothing length, h , of the SPH particles in the test disc initially.

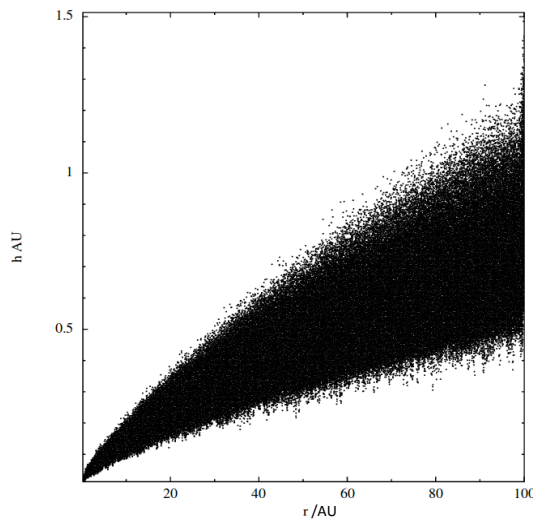


Figure 3.5: Smoothing length (h) of the SPH particles in a high mass disc as a function of radius (given in AU). As the density of the disc increases with radius on the midplane, the smoothing lengths of the particles also increases. The diagram shows that particles very close to the star have small smoothing lengths which cover a narrow range of values, but particles at large radii from the star tend to have larger smoothing lengths in general and a much larger range of values.

3.8 Summary

In this chapter we discussed how we set the disc density and temperature profiles. We assume that the density drops as $\sim R^{-p}$ and the temperature as $\sim R^{-q}$ with the distance from the central star, where the typical values for p and q are 1 and 0.5, respectively. The disc density also drops in the vertical direction, away from the midplane. We used random numbers to distribute particles in the disc so as to match the assumed density profile. The disc velocity profile is assumed to be Keplerian, i.e. the centripetal force on a mass element at a given radius is provided by the gravity of the central star and the gravity of disc within that specified radius.

Chapter 4

Testing the Code

4.1 Disc Set Up

We test the code by running simulations with similar initial conditions with Ayliffe & Bate (2010) – AB2010. We simulate the evolution of a Jupiter mass planet embedded in disc around a $1 M_{\odot}$ star. The disc has an inner radius of 0.52 AU, an outer radius of 15.6AU and a mass of $0.005 M_{\odot}$. A Jupiter mass planet is placed at 5.2 AU from the central star. Unlike the AB2010 model we did not have a potential barrier to prevent accretion onto the planet. Accretion occurred onto the planet, thus changing the planet mass over time.

4.1.1 Disc Surface Density Profile

The disc surface density profile is set using

$$\Sigma(r) = 2.2 \times 10^{-4} \left(\frac{r}{r_0}\right)^{-1} M_{\odot} \text{AU}^{-2} \tag{4.1}$$

4.1.2 Temperature Profile

AB2010 uses a local isothermal and a radiative hydrodynamic (RHD) method to model their discs. In order to test our code we also use the local isothermal approximation and then compared this to a radiative transfer method of Stamatellos et al. (2007) The temperature profile that we use is:

$$T_d(R) = \left[300^2 \left(\frac{R^2 + R_0^2}{AU^2} \right)^{-0.5} + 10^2 \right]^{1/2} \text{ K} \quad (4.2)$$

where $R_0=0.52$ AU.

In our disc there are no ghost particles around the outer edge of the disc (at 15.6 AU). In the AB2010 disc these particles added a second pressure barrier to the disc to stop the disc from spreading due to viscosity. Any particles which did pass through this barrier are then removed from further calculation. In the case of our test disc, there is no such barrier and as such particles can move beyond the initial outer edge of the disc and they are still be considered to be part of the disc. In these simulations, as in AB2010, we used 2×10^6 particles as it gives a good balance between resolution of the detail within the disc and the speed with which the simulation runs.

4.2 Relaxing the Disc

Before placing the planet into the disc, the disc is allowed to “relax” (Figure 4.1) i.e. to evolve for approximately 180 yr which is equivalent to three complete orbits of the disc outer edge. After the relaxation period a planet of one Jupiter mass is added to the disc at an initial radius of 5.2 AU. We then allow the disc to evolve for a further 2000 yr or approximately 170 orbits of the planet. In order to accurately compare our disc to the AB2010 disc, we will compare migration rates during the first 50 orbits, once the planet has settled into the disc.

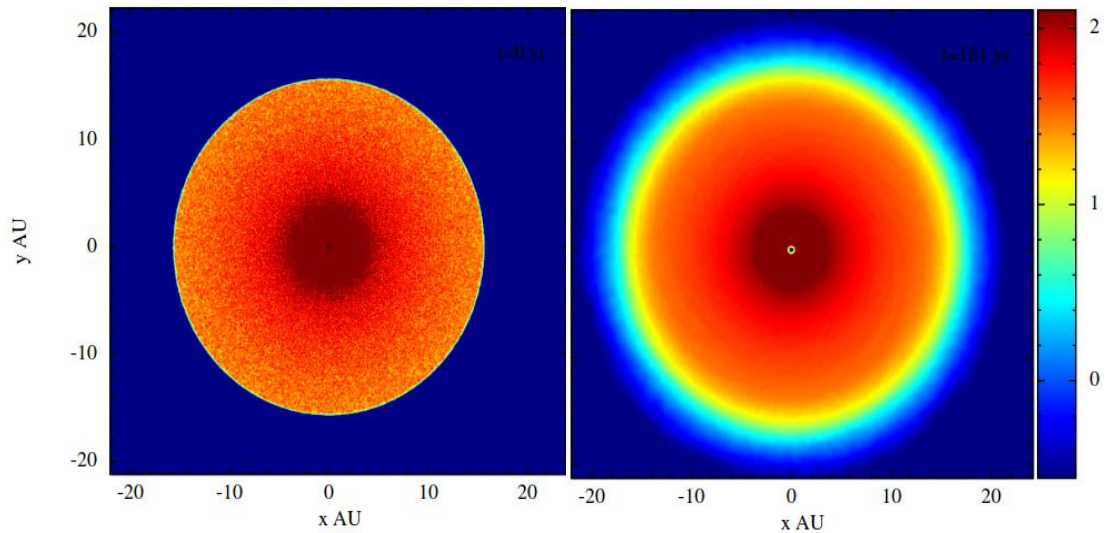


Figure 4.1: The plot above shows the initial logarithmic surface density (in units of g cm^{-2}) of the Ayliffe & Bate (2010) disc and the one on the right shows the surface density of the disc after the outer edge has completed three orbits. We then add a planet to the relaxed disc. This disc was evolved using the local isothermal model. The initial disc, as set up from our initial conditions (left) has an artificial looking very defined edge. In the image on the right, once the disc has evolved, the edges are more diffuse and the change in density is more gradual, as shown by the colour gradual change in colour. This represents a more natural disc.

4.3 Comparing simulations

In AB2010 the planet is modeled in three ways. Firstly using a sink, for which any particles that come within a set radius of the planet would be simply removed from the calculations; secondly, using a treatment which creates a surface force on the planet and thereby allows particles to pile up on the surface of the planet, and thirdly, the method we use in our simulations, an accreting sink particle. This way the planet grows in mass and corresponds more appropriately to the behaviour of a real planet within a gaseous disc.

Figure 4.2 shows the logarithmic surface density plots of the two simulations that we have performed. Both have the parameters as set out in AB2010 however the temperature profiles are different for each. The left column uses a local isothermal model (as in AB2010) and the right column uses a radiative transfer model (Stamatellos et al 2007). Initially both discs evolve in a similar way but after 625 yr it is clear that the orbital periods of the two planets are not the same. After 2000 yr the gap formed by the planet in the RT disc is far more pronounced than the gap in the local isothermal disc, as in the RT case the disc is cooler. The density around the star is less in the RT disc and there are finer ripples within the disc itself.

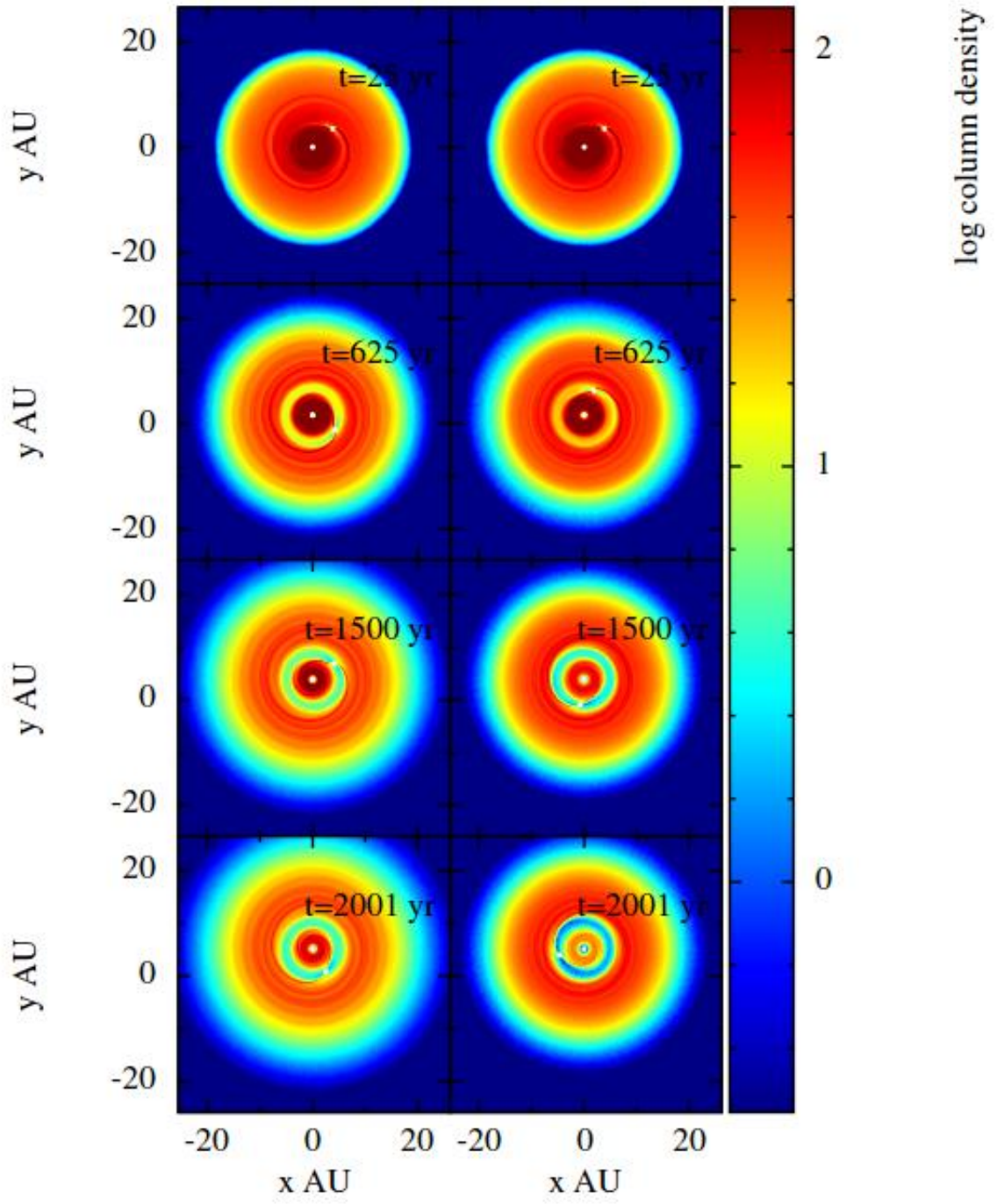


Figure 4.2: The images show the surface density of the disc after 25 yr, 625 yr, 1500 yr and 2001 yr after the planet has been added. The column to the left shows the local isothermal model and that to the right shows the radiative transfer model. In this simulation the RT model does not include the radiative heating from the star. After 2001 yr the RT run shows the planet has opened up a more defined gap and had therefore removed more of the disc from its orbital path. The wakes of the planet are more refined in the RT models than in the local isothermal model. The local isothermal disc also becomes more extended over time.

4.4 Migration

The change in the orbital radius and the semi-major axis of the planets in the two test runs are shown in Figures 4.3 and 4.4. The planet migrates further inward in the RT case (green line). In order to calculate the migration rate of the planet we must compare the final semi-major axis of the orbit with the initial semi-major axis of the orbit. This allows us to calculate the average migration timescale of the planets, τ . According to Ward (1997) and Tanaka et al. (2002), τ should have a value of between 10^4 and 10^5 yr for Jupiter mass planets. When we calculate the average migration timescales of the radiative transfer method and the local isothermal method we get values of 0.25×10^5 yr and 0.51×10^5 yr, respectively.

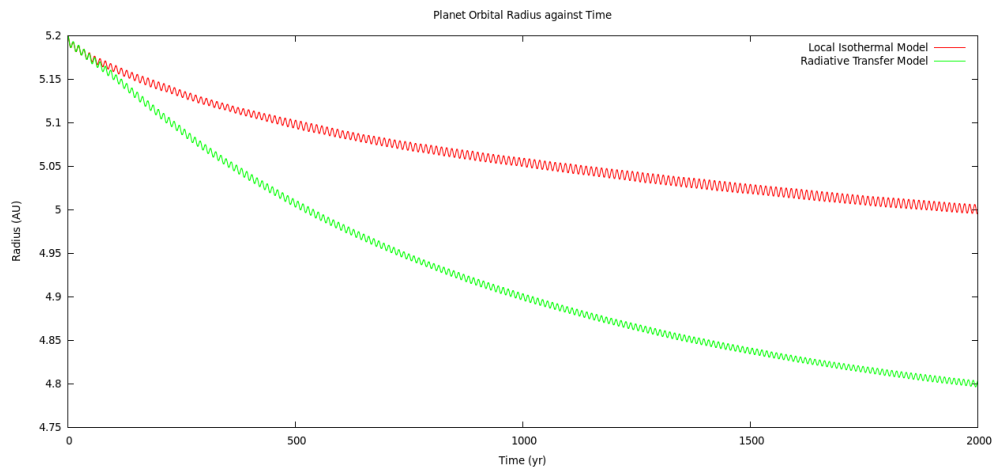


Figure 4.3: The planet orbital radius in the two runs with local isothermal shown in red and radiative transfer shown in green. The wobble which can be seen in each of the plots represents the eccentricity of the orbit. The rate of migration on the radiative transfer model is almost double that of the local isothermal model and therefore the total migration of the planet in the RT model is far greater.

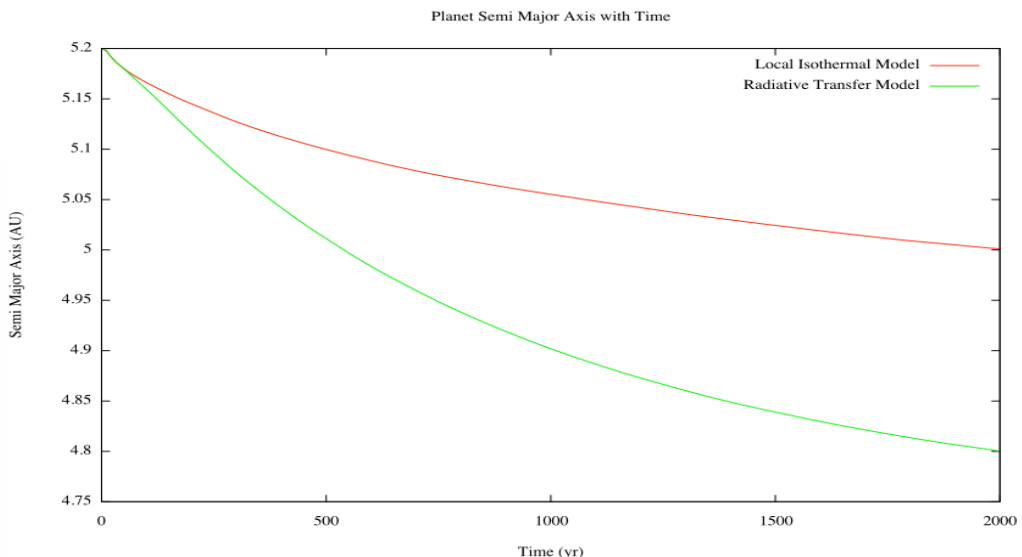


Figure 4.4: The semi-major axes of the planets in both the local isothermal and the radiative transfer methods with local isothermal shown in red and radiative transfer shown in green are plotted against time. In the local isothermal run the migration of the planet is slower than in the radiative transfer run despite both following the same rate of inward migration for the first few orbits. From the gradients of the curves we can see that at 2000 years the rate of migration of the radiative transfer run is still greater than that of the local isothermal case.

4.5 Eccentricity

As the planet migrates its orbital eccentricity increases (Figure 4.5). This eccentricity is a measure of how elliptical the orbit has become. In both the AB2010 run and the RT run, the eccentricity of the planet starts at zero (indicating a circular orbit) and then increases before settling into an ellipse with an eccentricity of between 0.0012 and 0.0014. This is not much greater than the eccentricity of the Earth and implies that these planets have an almost circular orbit. (The eccentricity of the orbit of the Earth is in the order of 4×10^{-4} which is considered to be an almost circular orbit).

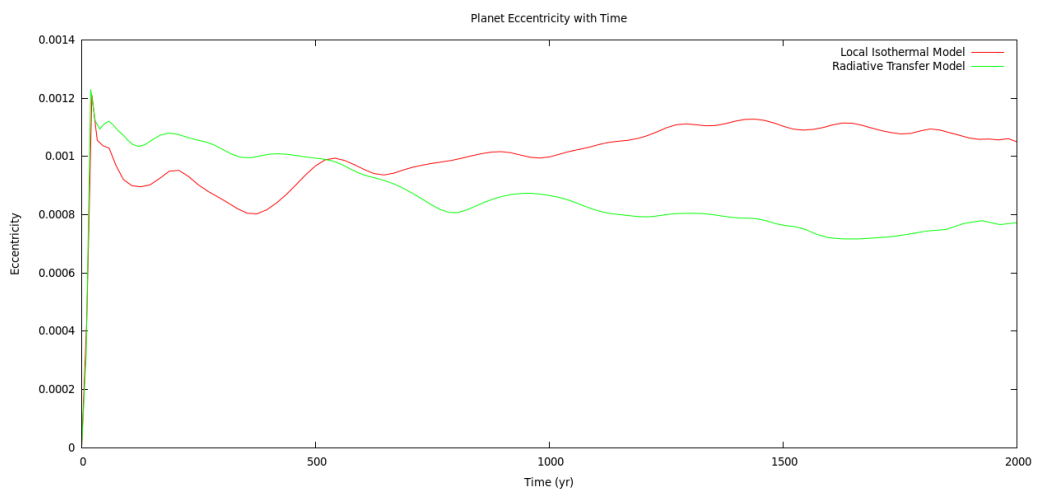


Figure 4.5: The eccentricity of the planets plotted against time for the two runs with the local isothermal model shown in red and the RT model shown in green. Despite following the same initial trend the local isothermal model shows generally less eccentricity than the radiative transfer model. These very low values of eccentricity could be very well by noise from the smoothed hydrodynamics itself.

4.6 Accretion

The rate of accretion onto the planet (shown in Figure 4.6 below) initially is large. In a disc a planet grows in mass by accreting gas from the disc in these simulations, a sink particle is placed within the disc representing an already formed planet with 1 Jupiter mass. During the first several orbits this planet carves its way through the disc accreting any matter which is in its path.

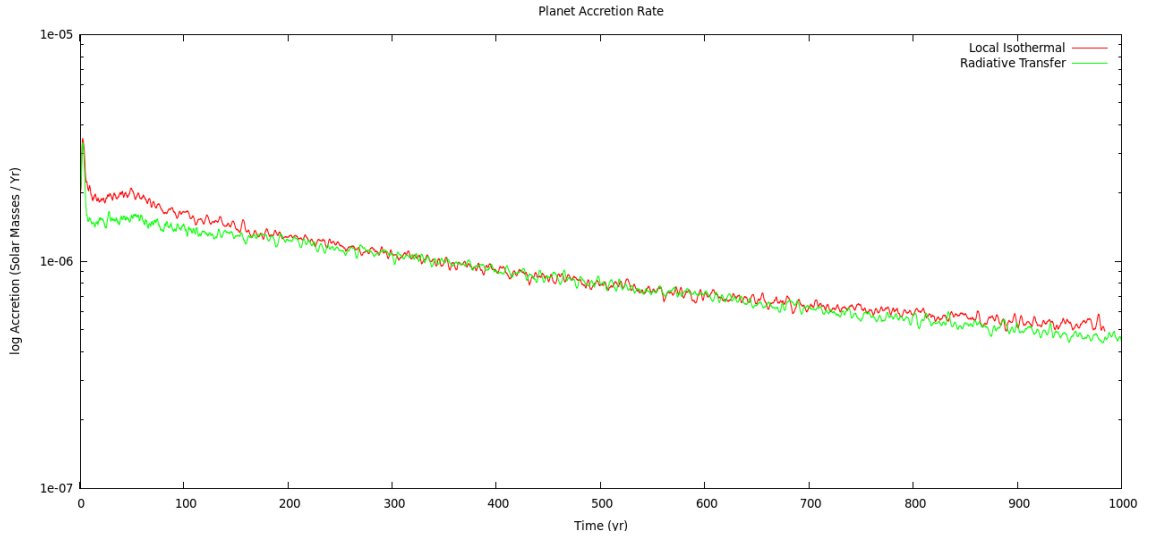


Figure 4.6: Accretion rates on the planets of the two test runs with local isothermal shown in red and the RT run shown in green. The general trend of accretion in each case is similar with the rate of accretion onto the planet in the local isothermal method being slightly higher overall.

4.7 Comparison with Ayliffe and Bate 2010

By comparing the results of the simulations presented in this chapter with the migration timescales obtained in AB2010 (Table 4.1) we can ascertain whether or not our code reproduces previous results, and therefore whether it is appropriate for the study of planet migration.

The average migration timescales and migration rates are calculated at different times during the evolution of the system using the semi-major axis the planet (see Table 4.1 below) from my results.

Time (yr)	475	525	875	925	1475	1525	1875	1925
	α_1 (AU)	α_2 (AU)	α_3 (AU)	α_4 (AU)	α_5 (AU)	α_6 (AU)	α_7 (AU)	α_8 (AU)
Local Isothermal	5.10	5.10	5.06	5.06	5.03	5.02	5.01	5.00
Radiative Transfer	5.02	5.01	4.92	4.91	4.84	4.84	4.81	4.81
	τ_1 (yr)		τ_2 (yr)		τ_3 (yr)		τ_4 (yr)	
Local Isothermal	3.7×10^4		6.0×10^4		8.8×10^4		1.1×10^5	
Radiative Transfer	1.9×10^4		2.5×10^4		4.8×10^4		8.8×10^4	
	$m1$ (M_j)		$m2$ (M_j)		$m3$ (M_j)		$m4$ (M_j)	
Local Isothermal	1.66		1.94		2.25		2.42	
Radiative Transfer	1.61		1.87		2.12		2.23	

Table 4.1: Table 4.1 shows the semi major axis (α), migration time scale (τ) and mass of the two planets in each of the runs at or between specific times in each simulation. By taking two values of α , the migration timescale can be calculated between those two points. The larger the migration timescale the slower the migration of the planet. We do not take very early values of migration timescale into account here as the planet has been placed in the disc rather than organically forming there which means that the opening of a gap for planet will produce and unnaturally rapid migration.

The values of migration timescales for the two local isothermal treatments are similar (9-11) $\times 10^4$ yr for AB2010 and (3.71-10.6) $\times 10^4$ yr for our local isothermal run. The radiative transfer simulation produced a wider range of migration timescales but the migration timescales are consistent with the values obtained in AB2010. The migration rates of planets in the two local isothermal runs are very similar to the ones from AB2010 suggesting that our method/code is reliable.

	AB2010 Local Isothermal	AB2010 Radiative transfer (Taken from a Graph)	Local Isothermal	Radiative Transfer
Migration Timescale (yr)	(9-11) $\times 10^4$	1.5 $\times 10^4$	(4-11) $\times 10^4$	(2-9) $\times 10^4$

Table 4.2: Migration timescales of both simulations presented in this chapter and the values obtained in AB2010. The values we obtain are comparable with the ones from AB2010, which suggests that our code is reliable. Our radiative transfer values are likely different to those in AB2010 due to the increase in planet mass over the course of the run. In the AB2010 RT run the planet mass remained fixed at the initial mass which causes a change in migration timescale overall.

4.8 Summary

After running two test simulations using the parameters laid out by Ayliffe and Bate (2010), our similar rates of migration and migration timescales suggest that our code is both suitable and reliable for planet migration studies. AB2010 find values of migration timescale for their local isothermal model of between 9 and 11 $\times 10^4$ yr. In our simulations our migration timescales ranged from between 3.71 and 10.6 $\times 10^4$ yr. These differences are likely due to the different type of the sink particles used in AB2010 and this paper. The AB2010 model uses killing sinks, in which any particles which enter the radius of the sink are removed from the simulation, and we use accreting sinks, in which any particles which enter the sink radius have their mass added to that of the sink. This difference in the mass of the planets over the course of the run will give rise to slightly different interactions between the planet and the disc.

Chapter 5

Giant Planet Migration in Massive Discs

The discovery of gaps in the disc of HL Tau (ALMA Partnership, 2015), a young pre-main sequence star still embedded in its parent envelope, opens up the possibility that planets form early on during the lifetime of a protostellar disc, while the disc is still relatively massive. In this Chapter we will examine the migration of giant planets in massive discs.

5.1 Setting up the discs

We produce two different discs in order to compare the migration of planets placed within them. Both discs are represented by 2×10^6 particles and the masses of the discs are set to be $0.07 M_{\odot}$ and $0.1 M_{\odot}$, respectively. Each disc is evolved for 3000 yr before a planet is placed into it at 40 AU initial orbiting radius or 80 AU initial orbital radius (Figure 5.1). We therefore examine a total of 4 cases (see Table 5.1). At these initial radii, planets in real protoplanetary discs could form due gravitational fragmentation (Rice 2004). The orbits of the planets are initially circular. We use accreting sinks for both the star and the planet and set the masses of the sinks to be $1 M_{\odot}$ and $1 M_J$, respectively. The disc surface density profile is set using:

$$\Sigma(r) = 3.2 \times 10^{-4} \left(\frac{r}{r_0}\right)^{-1} M_{\odot} \text{AU}^{-2} \quad (5.1)$$

We use the radiative transfer model of Stamatellos et al. (2007) and set the pseudo-background temperature profile as:

$$T_d(R) = \left[T_0^2 \left(\frac{R^2 + R_0^2}{\text{AU}^2} \right)^{-0.5} + 10^2 \right]^{1/2} \text{ K} \quad (5.2)$$

The original disc has a radius of $R=100$ AU with a softening radius set to $R_0=0.25$ AU. The temperature at 1 AU is set to $T_0=250$ K.

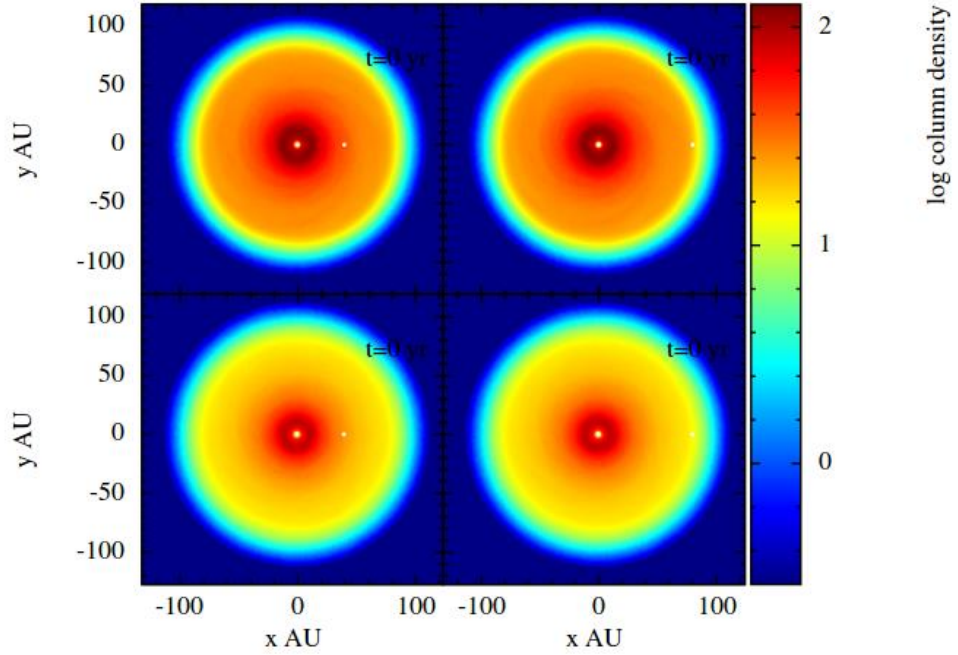


Figure 5.1: The initial logarithmic surface density profiles of all four discs as a planet is added to them (units g cm^{-2}). The planets on the bottom row are of the $0.07 M_{\odot}$ disc and those on the top row are of the $0.1 M_{\odot}$ disc. The left two plots are of planets initially placed at 40 AU and the right two plots are of planets initially placed at 80 AU.

Run ID	Disc mass (M_{\odot})	Planet mass (M_J)	Planet initial radius (AU)
Run 1	0.1	1	40
Run 2	0.1	1	80
Run 3	0.07	1	40
Run 4	0.07	1	80

Table 5.1: The initial parameters of all four runs and how they will be referred to from this point onwards.

5.2 – Planet migration within a 0.1- M_{\odot} disc

5.2.1 Surface Density

The density profiles of the two discs show a marked difference in evolution when a planet is placed at 80 AU rather than at 40 AU (Figure 5.2). In both cases the planet migrates inwards. The 80 AU planet opens a gap in the disc that widens quicker than the gap formed by the 40 AU planet and the width of the gap in the disc with the 80AU planet is also wider after 15000 yr. After 5000 yr the disc with the planet at 80 AU also shows fewer regions of high density beyond the inner disc, with the disc with planet at 40 AU.

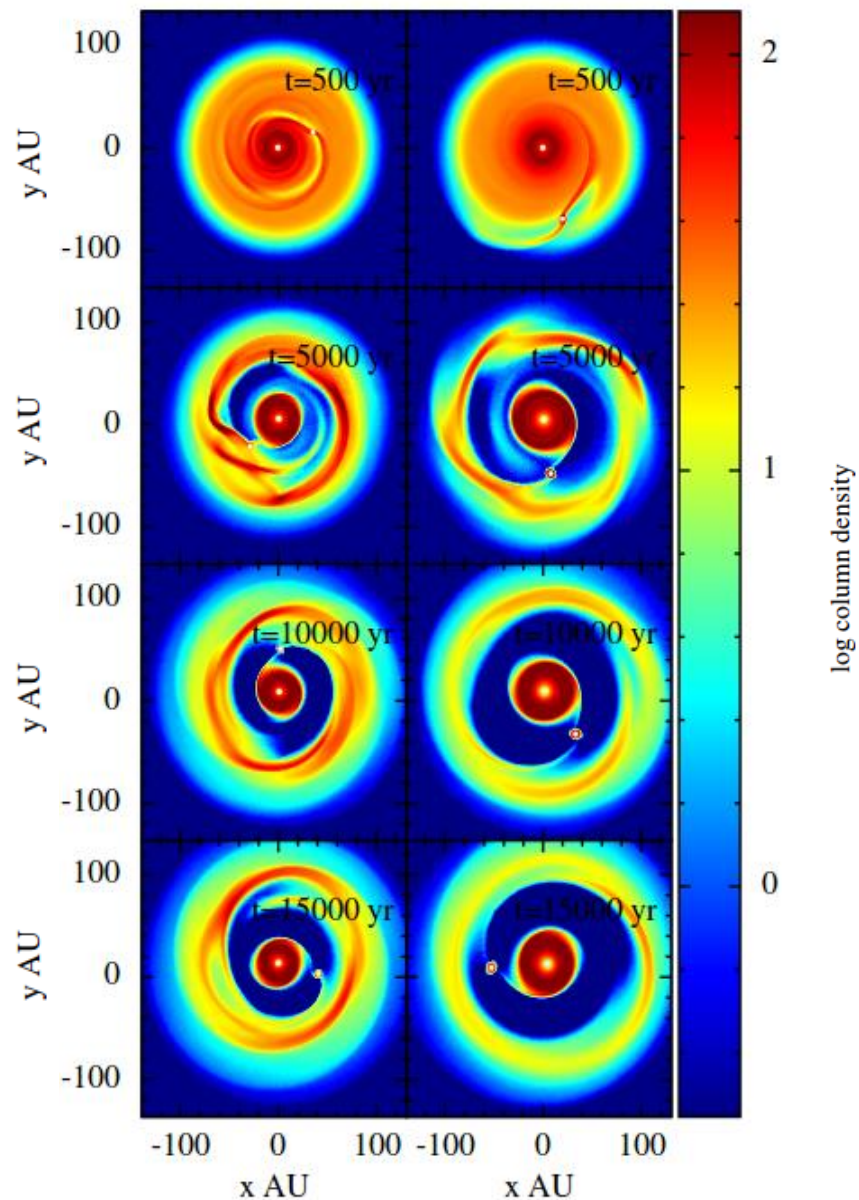


Figure 5.2: The logarithmic surface density of the 0.1 M_{\odot} mass disc with the planet initially placed at 40 AU to the left and the planet initially placed at 80 AU on the right (in units g cm^{-2}). The density variations of the disc are apparent on the plots of the planet initially at 40 AU. Spiral arms can be seen with most prevalence at around 5000 yr. The gap opened by the planet at 80 AU is much wider than the gap opened by the planet at 40 AU.

5.2.2 Migration within the 0.1- M_{\odot} disc

Initially we compare the migration of a planet placed at different initial orbital radii within two discs of the same parameters. Within the 0.1 M_{\odot} disc the planet initially at 80 AU shows a rapid inward migration within the first 3000 – 4000 years. The inward migration of the planet at 40 AU is not as fast and after approximately 2000 yr this planet undergoes slight outward migration before apparently stabilising at an orbit just beyond its original orbital radius (see Figure 5.3).

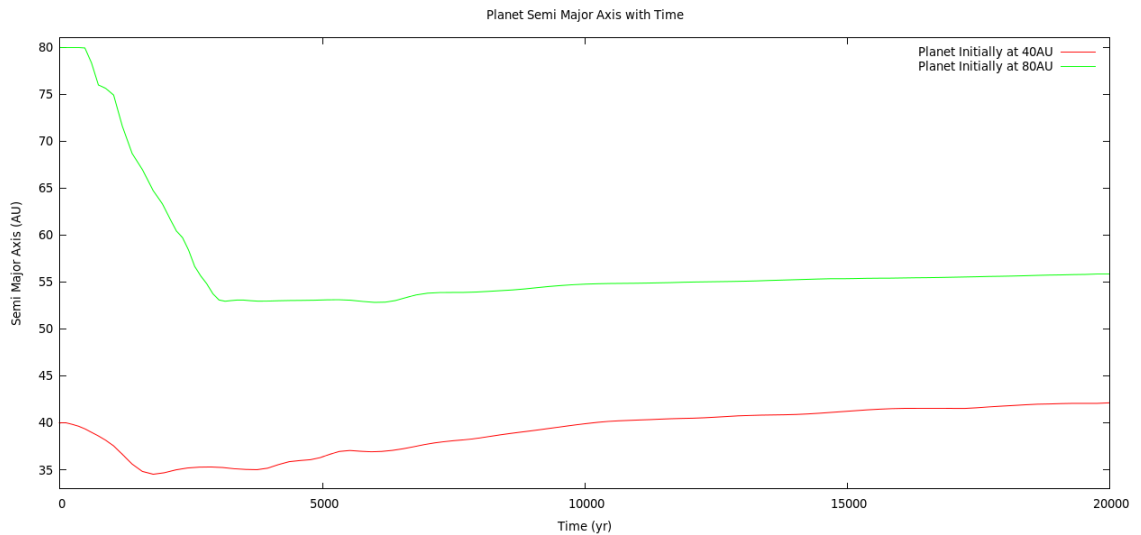


Figure 5.3: The semi-major axes of the two planets within the 0.1 M_{\odot} disc shows initial inward migration for both planets. The 80 AU planet (shown in green) has an initial rapid migration and then settles into a stable orbit. The 40 AU planet (shown in red) initially migrates inwards before starting migrating outwards throughout the rest of the run.

By looking at the orbits of the two planets (in Figure 5.4) it is clear that the 80 AU initial orbital radius planet, despite a large initial inward migration, settles into an almost circular orbit at around 55 AU.

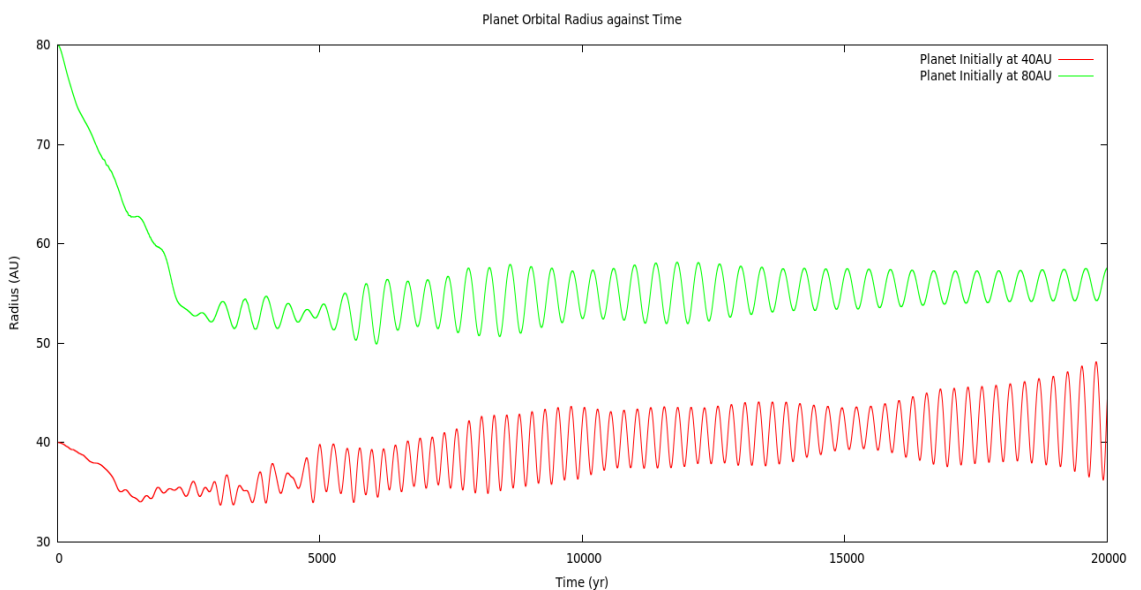


Figure 5.4: Orbital radii of the two planets within a 0.1 M_{\odot} disc. The undulations in the radius indicate the eccentricity of the orbit and whilst these decrease for the 80 AU initial orbital radius planet (shown in green), the 40 AU initial orbital radius planet shows an increase in the eccentricity.

5.2.3 Eccentricities of planets within the 0.1 M_⊙ disc

The eccentricities of the two planets within this massive disc are very different over the course of the 20,000 yr for which we simulate the disc (Figure 5.5). The 80 AU initial orbital radius planet settles into a stable orbit with an eccentricity of around 0.03. The 40 AU initial orbital radius planet (displayed in red in Figure 5.5 below) shows a very rapid increase in eccentricity especially during the final 5000 yr.

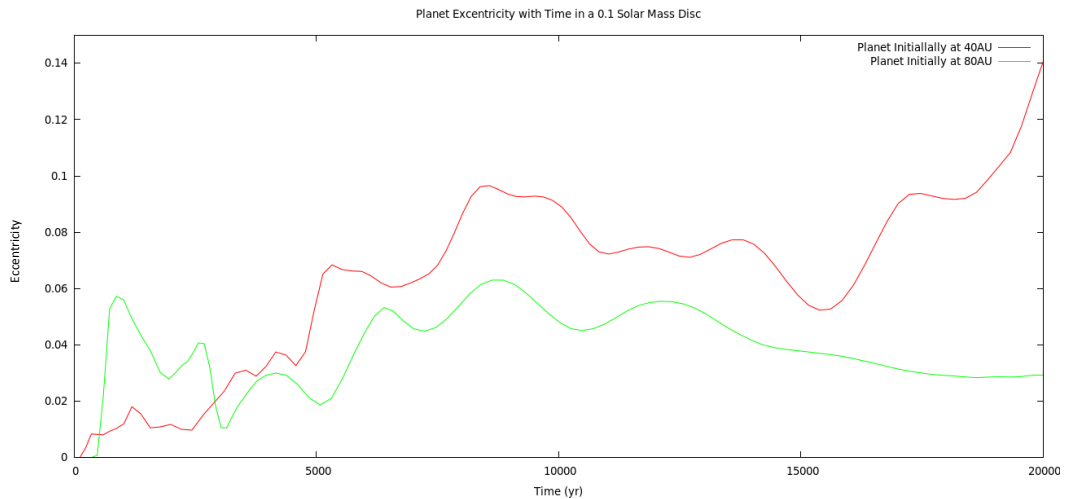


Figure 5.5: The eccentricities of the two planets within the 0.1 M_⊙ disc. The planet initially at 40 AU (shown in red) shows an eccentricity of 0.14 AU after 20 kyr. The decreasing and then almost constant eccentricity of the 80 AU initial orbital radius planet (shown in green) shows that it settles into a nearly circular orbit.

The masses of the two planets both increase due to accretion as they move through the disc (Figure 5.6). The initial stages of this accretion should not be considered as being representative of a realistic planetary disc as the sink particles are artificially placed within a disc rather than being allowed to form self-consistently by one of the methods outlined in Chapter 1. The levels of accretion seen initially are caused by the planet carving out a gap during its first few orbits.

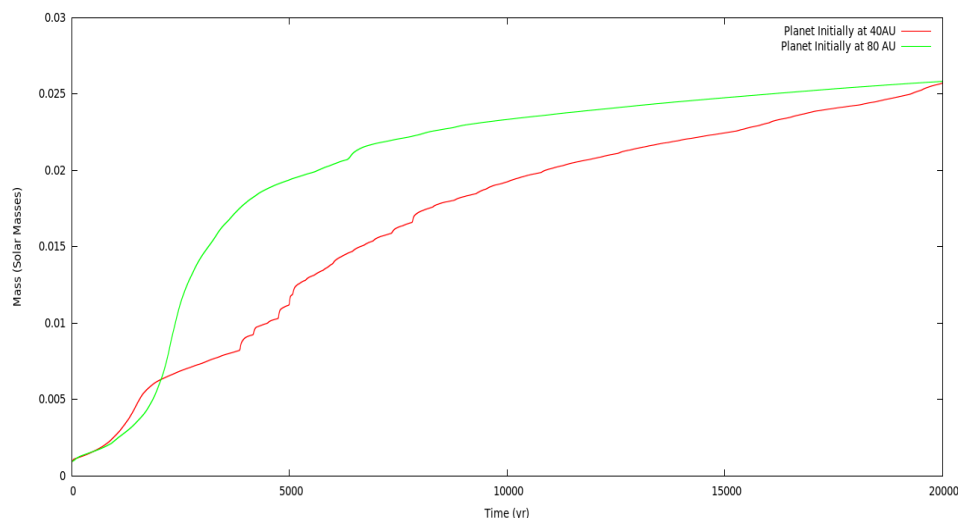


Figure 5.6: The masses (in M_⊙) of the two planets with the planet initially at 40 AU shown in red and the planet initially at 80 AU shown in green. Coincidentally both planets are the same mass after 20 kyr despite very different patterns of accretion. The pattern of the mass increase on the 40 AU planet indicates interactions with the disc as the bumps in the line indicate matter is added to the planet in bursts rather than a steady trickle. This is likely due to the areas of high and low density that the 40 AU initial radius planet passes through – see figure 5.8.

The accretion on both planets follows similar patterns (Figure 5.7). However, the 80 AU initial orbital radius planet is rapidly migrating inwards and takes more time to open up a gap with peak accretion taking place at around 2.5 kyr. The 40 AU initial orbital radius planet accretes relatively large amounts of mass in bursts, the largest of these occurs at 5 kyr. Despite these very different accretion profiles (Figure 5.7) after 20 kyr both planets have the same final mass. This is purely by coincidence. (In the $0.07 M_{\odot}$ disc the two planets show very different masses after 20000 yr, see Section 5.2). The peaks in the accretion rates are likely caused by the interaction with spiral arms that have formed in the disc due to its massive nature (Figure 5.8). The distance between the peaks coincides with the orbital period of the planet suggesting that once every orbit it interacts with an area of relatively high density which deposits a larger amount of matter onto the planet.

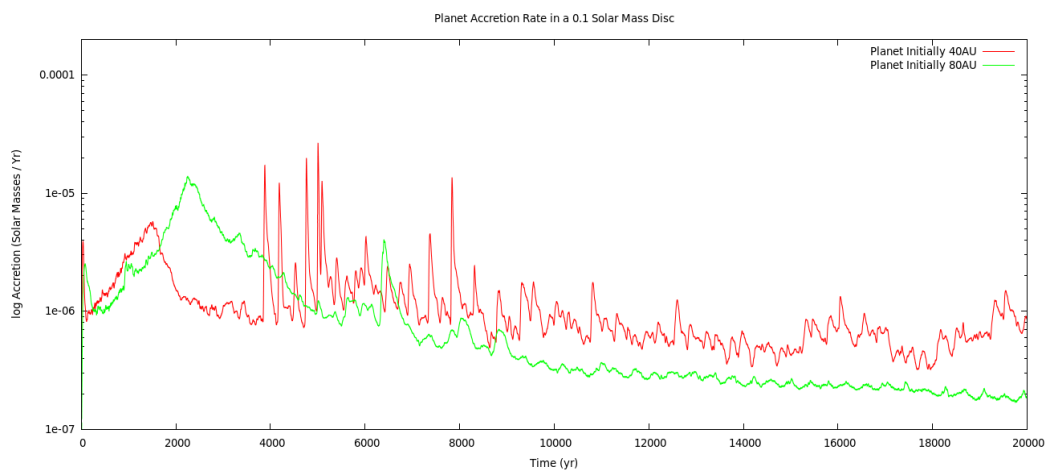


Figure 5.7: The accretion rates onto planets in the two simulations. The initial peak (around 2.5 kyr) of the accretion rate onto the planet initially at 80 AU (shown in green) is caused by the rapid inward migration of the planet gaining access to fresh material as it moves through the disc. The peaks seen in the planet initially at 40 AU are caused by interactions with the wakes of the planet moving through the disc shown in Figure 5.8 below.

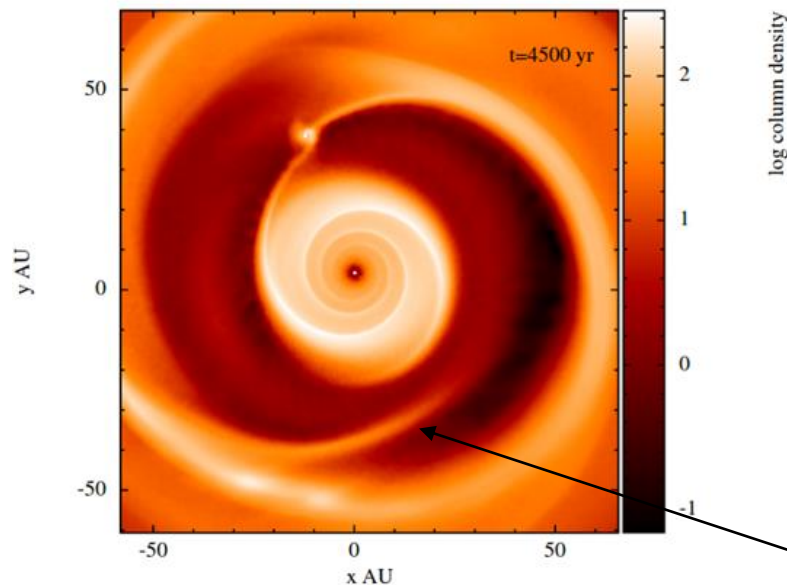


Figure 5.8: The inner region of the $0.1M_{\odot}$ disc with a planet originally placed at 40 AU. The wakes caused by the planet moving through the disc can clearly be seen (indicated by the arrow), including an area of high density which intercepts the orbit of the planet causing increased accretion and sudden bursts of new mass being added to the planet as shown by the bumps in the line on the graph in figure 5.6.

Initially the accretion rate onto the star in the $0.1 M_{\odot}$ disc (Figure 5.9) follows the same pattern of decrease for both runs, however at around 2.5 kyr the rate of accretion on the star from the disc in which the planet is initially at 40 AU remains high and even increases halfway through the run. Due to the proximity of the 40 AU initial orbital radius planet to the star, it can drive accretion onto the central star.

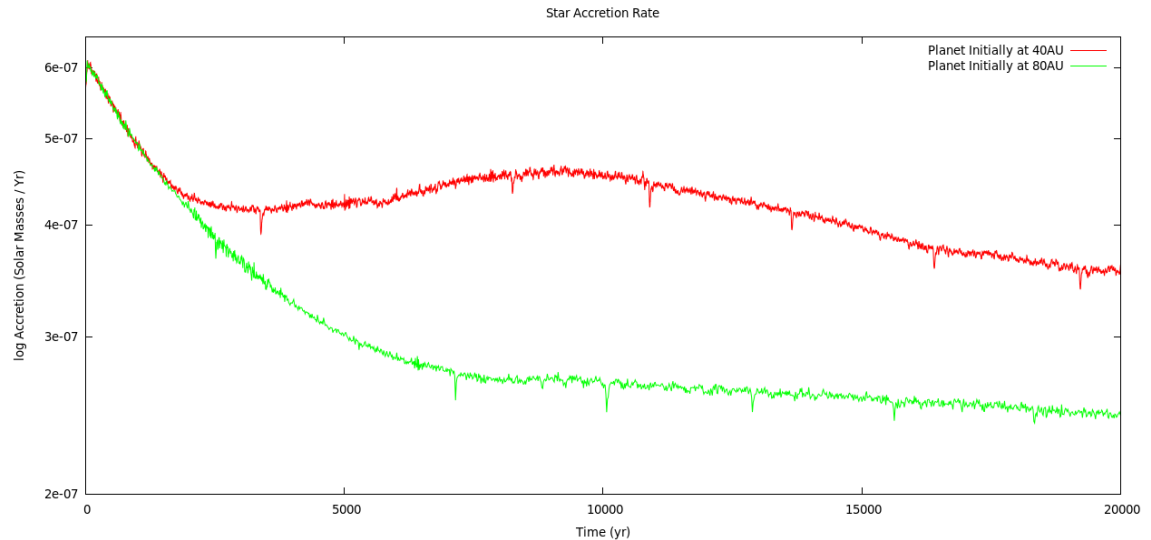


Figure 5.9: Accretion onto the star in the $0.1 M_{\odot}$ disc with the planet initially at 40 AU shown in red and the planet initially at 80AU shown in green. The perturbations in the disc caused by the closer orbit of the 40 AU initial orbital radius planet cause more material to be accreted onto the star and the planet in closer proximity drives accretion as it forces matter inwards with its wake. The accretion onto the star in the disc of the planet initially at 80 AU continues to decrease throughout the course of the run.

5.3 – Planet migration within a $0.07 M_{\odot}$ disc

We now examine the migration of planet within a lower mass disc, i.e. with a mass of $0.07 M_{\odot}$ (Figure 5.10). The way that planets within a 0.07 solar mass disc (Figure 5.10) alter the disc's evolution is markedly different depending on the location of the planet within the disc. At 5000 yr the planet at 80 AU has already opened a gap in the disc (although it is not fully formed yet) whereas at the same time interval the planet at 40 AU has had a far less dramatic impact on the disc's structure. Between 10,000 yr and 15,000 yr in both runs there is not a significant difference in the appearance of the disc, suggesting that it has reached a steady state and not much migration takes place. The 80 AU planet disc, has expanded considerably beyond its initial 100 AU and has a less dense and less compact central region. The 40 AU planet disc has a region of high density outside the gap opened up by the planet.

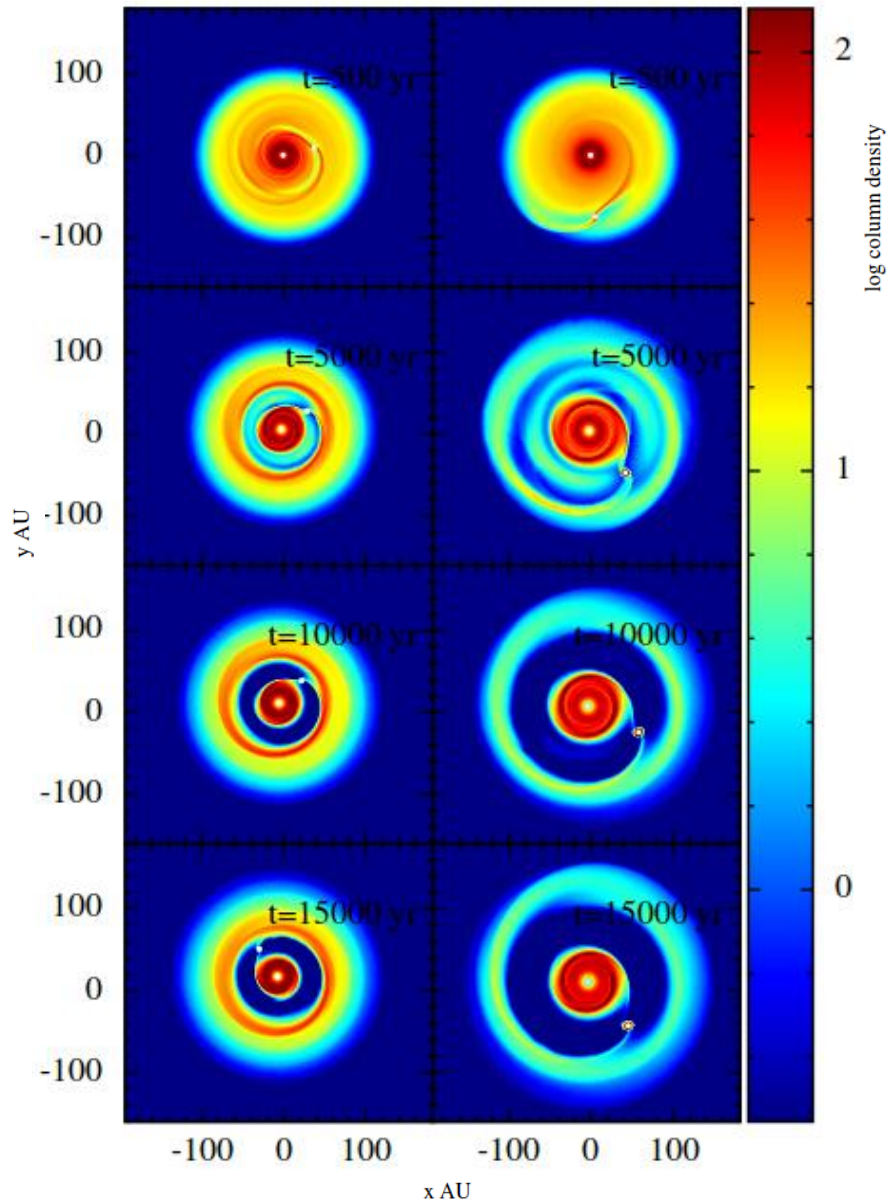


Figure 5.10: Logarithmic surface density profiles (in g cm^{-2}) of the runs with a $0.07 M_{\odot}$ disc. The two planets show different behaviours. The plots on the right are of the planet initially placed at 80 AU and show that the planet opens up a very large gap between 5 and 10 kyr. The final density of the rest of the disc is also far lower than that in the disc with the planet initially at 40 AU. Unlike the planet initially at 40 AU in the $0.1 M_{\odot}$ disc strong wakes have not formed in this disc due to its smaller mass. The 80 AU planet disc has a far less dense, more diffuse disc exterior to the planet compared with the 40 AU planet disc.

Within the $0.07 M_{\odot}$ disc, the planet initially at 80 AU shows a rapid inward migration over the next 2,500 yr of the run (Figure 5.11). The 80 AU initial orbit planet then gradually migrates outwards until the end of the simulation. Over the 20 kyr of the simulation, the total inward migration of this planet is less than 10 AU. The planet with an initial orbital radius of 40 AU shows very small changes in its orbital radius throughout the simulation. Despite some minor fluctuations in the semi major axis of the planet its orbit remains stable at just under 40 AU.

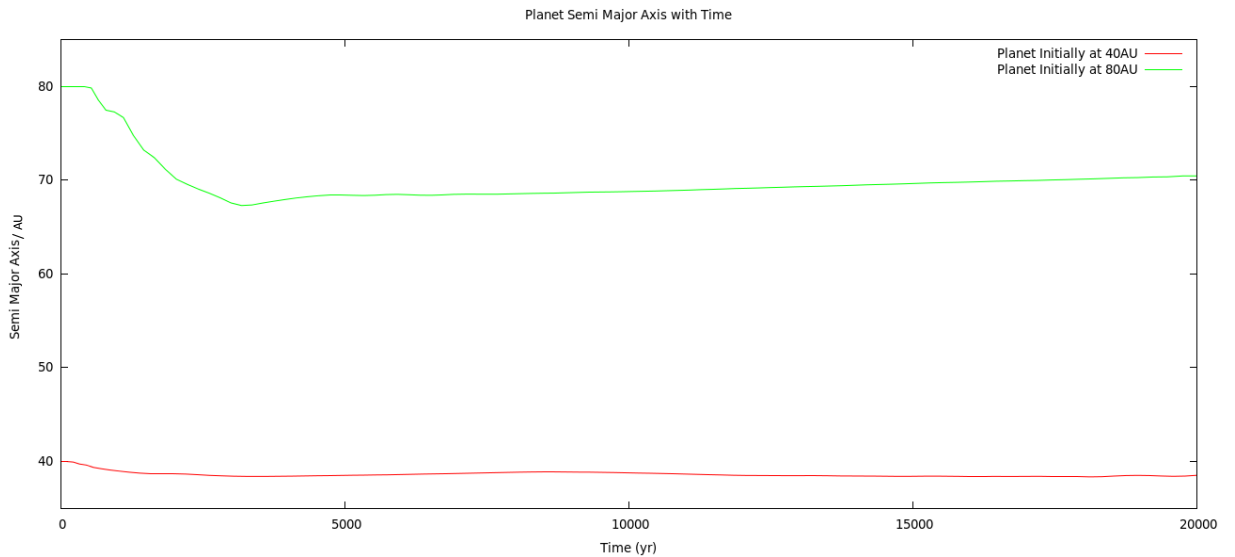


Figure 5.11: The semi major axes of the two planets over the duration of the runs. The planet initially at 80 AU (shown above in green) has rapid initial inward migration as it clears the disc in its immediate vicinity. Migration then becomes outward but slower. The planet initially at 40 AU (shown in red) has a total inward migration of about 2-3 AU.

In both runs the oscillations in their orbits increase over time suggesting both planets obtain a slightly more elliptical orbit (Figure 5.12). This is most pronounced in the planet initially at 40 AU.

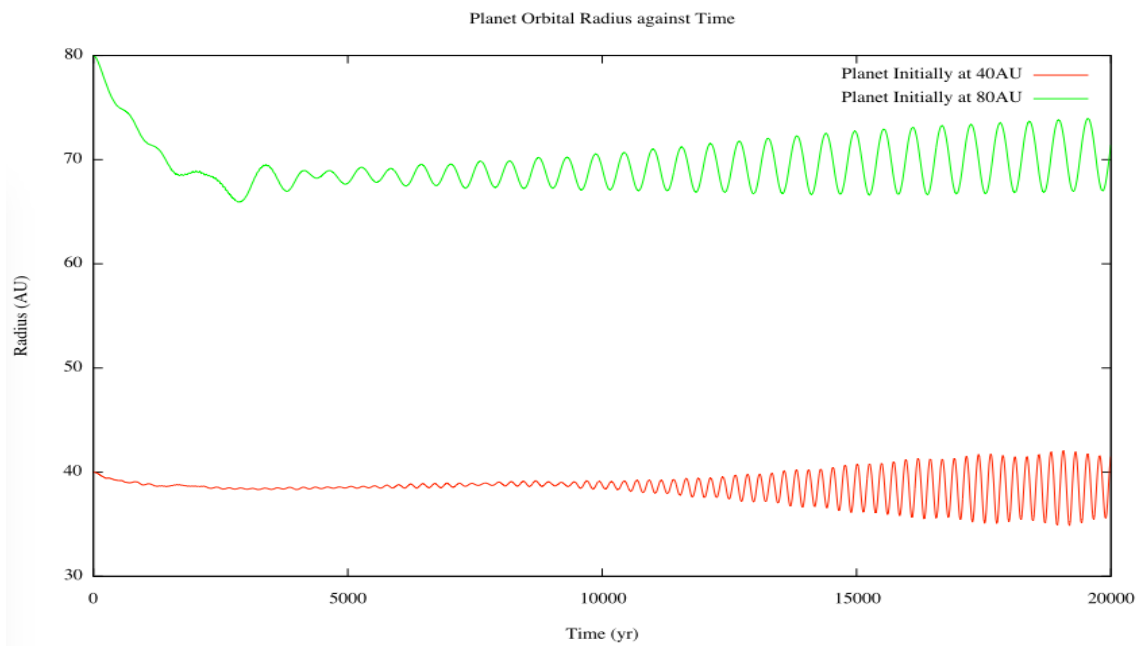


Figure 5.12: A comparison of the orbital radii of both planets when placed into a $0.07 M_{\odot}$ disc. The 40 AU initial orbital radius planet (red) shows greater undulations on the graph above. Overall the migration of the 40 AU planet is very minimal with almost no overall migration from its original 40 AU radius. The initial inward migration of the planet initially at 80 AU (green) can also be seen for the first 2-3 kyr of the simulation. The undulations in both lines represent the eccentricity of the planets.

When we compare the eccentricities (Figure 5.13) of the two planets there are peaks in the eccentricity of the planet initially at 80 AU for the first 5,000 yr. These are due to the relatively rapid inward migration experienced by this planet once it is established within the disc. The planet initially at 40 AU shows an exceptionally low value of eccentricity before rising relatively sharply to a value of approximately 0.08.

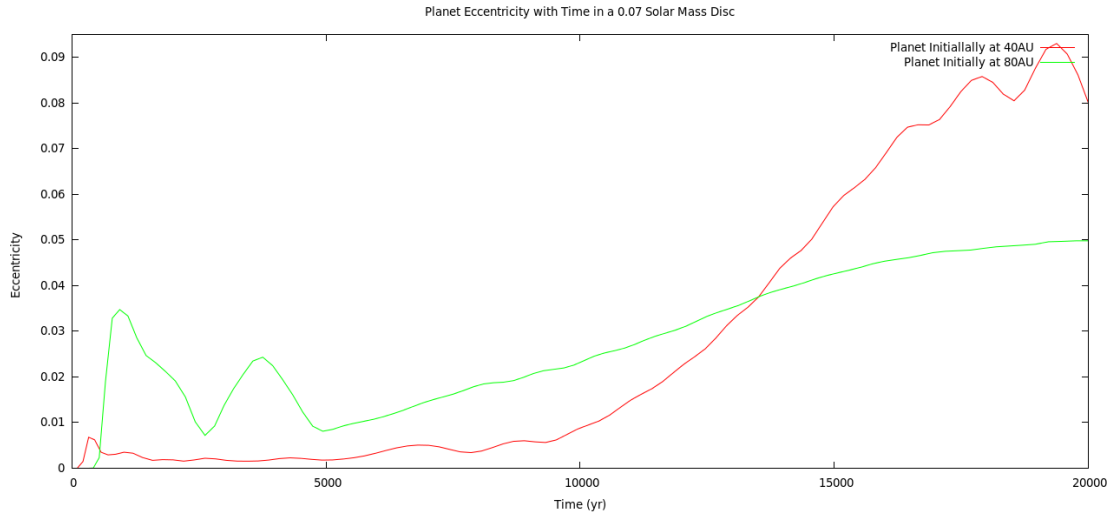


Figure 5.13: The eccentricities of the two planets in the lower mass disc with the planet initially at 40 AU shown in red and the planet initially at 80 AU shown in red. The 40 AU planet's eccentricity becomes relatively high after being exceptionally low for the first half of the run. Despite this rapid rise these are still low values for eccentricity and represent an almost circular orbit.

The masses of both planets (Figure 5.14) increase. The planet initially at 80 AU showing a much greater mass increase than the planet initially at 40 AU. As the planet at 80 AU initial radius is migrating inwards it is constantly encountering new material which accretes onto it. Due to the minimal migration of the 40 AU initial orbital radius planet it quite quickly accretes all the matter on its orbit and thereafter the accretion rate onto it slowly decreases.

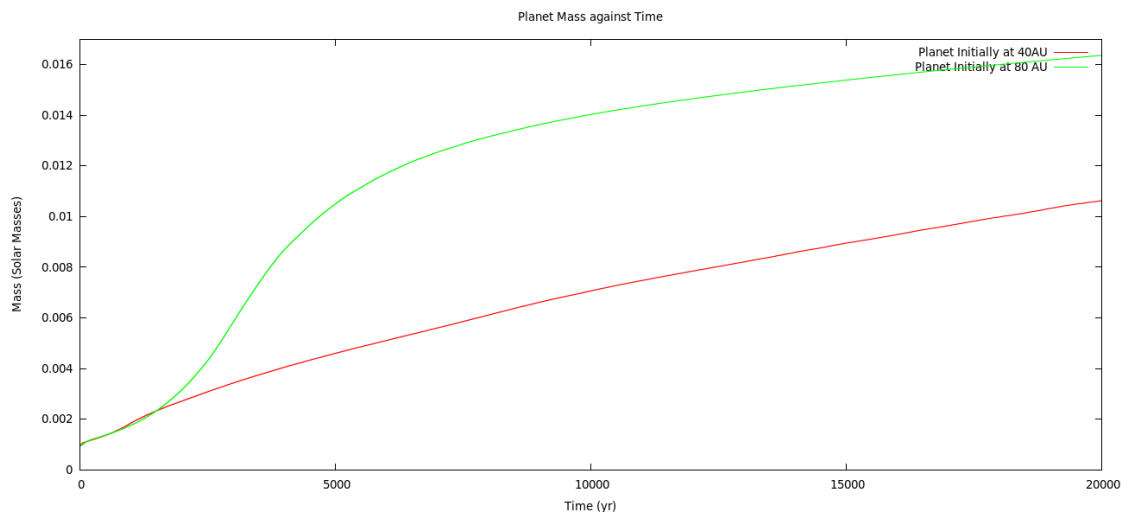


Figure 5.14: The increase in masses of the two planets over the course of the simulations. The increase in mass of the planet initially at 40 AU (shown above in red) is steady and has an almost constant gradient throughout. The 80 AU initial orbital radius planet has a rapid increase in mass between around 2,000-5,000 yr, before settling to a rate of mass increase very similar to that of the 40 AU initial orbital radius planet.

The accretion rates (Figure 5.15) show a large increase during the gap opening phase and then rapid decrease for the planet initially at 80 AU. This aligns with both the mass increase of the planet (Figure 5.14) and the migration of the planet (Figure 5.11). As the 80 AU initial orbital radius planet migrates inwards and carves through the disc it has access to more material than would have been available if no migration took place. As the 40 AU initial orbital radius planet does not migrate much, it does not have access to the larger amounts of disc material and therefore shows lower accretion rates (at least for the initial phases).

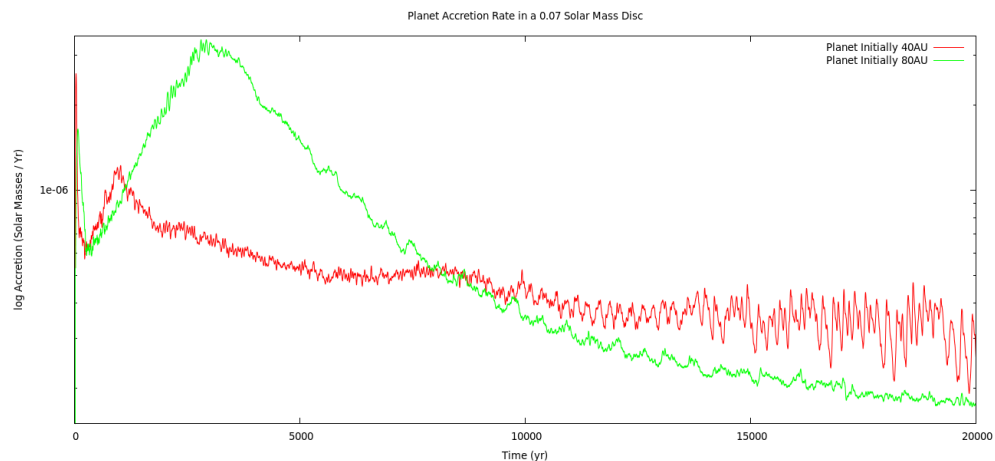


Figure 5.15: The logarithmic accretion rates of the planets within the lower mass disc with the planet initially at 40 AU shown in red and the planet initially at 80 AU shown in green. Both show artificially high rates of accretion at the very early stages of the simulation due to the planets being placed within a relaxed disc rather than being created within the disc. Over the first 3 – 4 kyr the 80 AU planet undergoes a very large accretion rate before steadily declining. The 40 AU planet has a much more erratic accretion pattern, especially over the last 5000 yr of the run.

In the $0.07 M_{\odot}$ disc (as with the $0.1 M_{\odot}$ disc) the pattern of accretion on to the star (Figure 5.16) is initially almost identical for both the planets initially at 80 AU and for the planet initially at 40 AU. The disc with the 40 AU initial orbital radius planet however maintains a relatively much higher rate of accretion onto the star. This is likely because the planet is driving accretion onto the central star due to its orbit being much closer to the star.

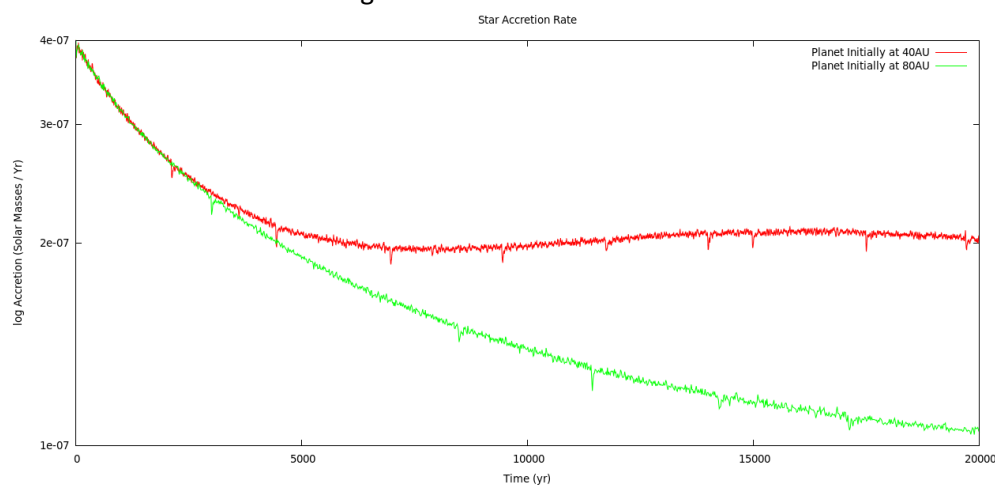


Figure 5.16: Accretion onto the star in the disc with a planet placed at 40 AU (shown about in red) is almost double that of the disc with a planet initially placed at 80 AU (shown above in green). As with the $0.1M_{\odot}$ discs the disc with the planet at a smaller orbital radius sustains a higher rate of accretion, likely due to the planet driving matter inwards towards the star.

5.4 - Comparison of the simulations of planet migration in massive discs.

We will refer to the simulations as outlined in Table 5.1. There are many similarities between discs in all simulations, however the evolved discs look very different after 20 kyr (Figure 5.19). The more massive discs have more evident spiral structure; this is especially the case in the Run1 disc where spiral arms are the more pronounced. In the lower mass discs, Run4 opens a huge gap as it migrates inwards. The gap opened by the Run3 planet is considerably smaller as the planet barely undergoes any migration and therefore cannot accrete much gas.

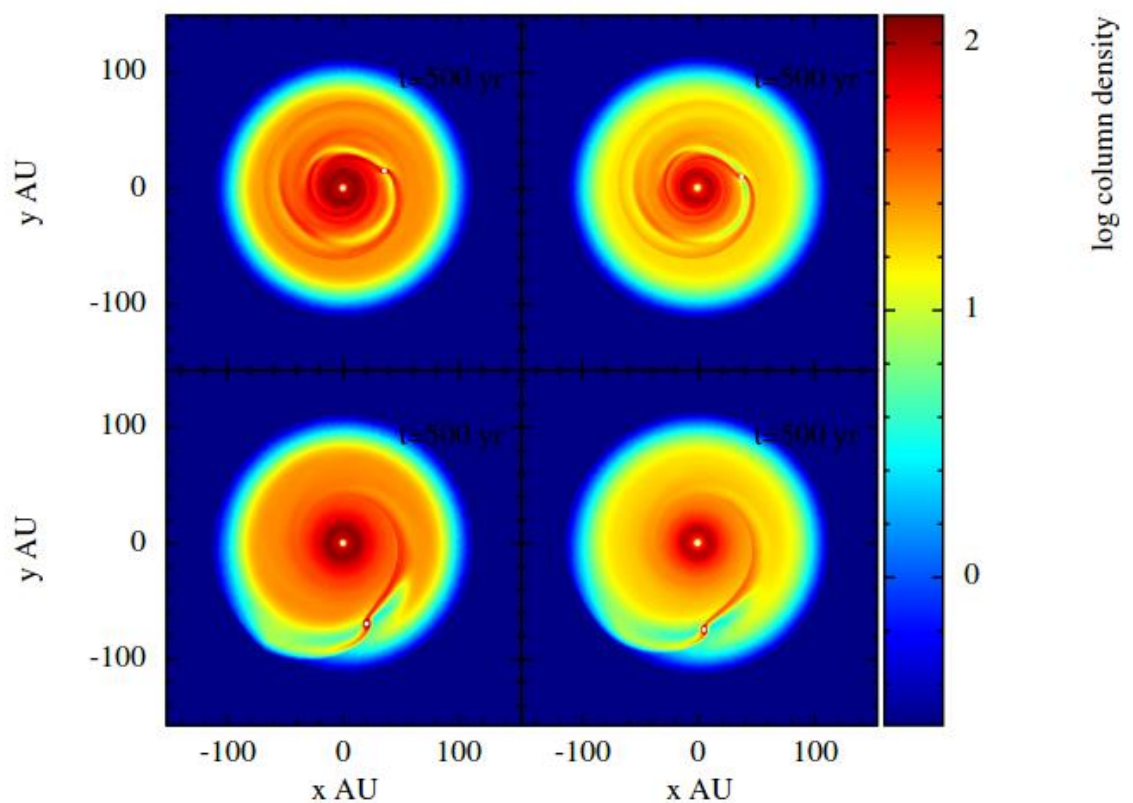


Figure 5.17: Surface density plots of the four simulations after 500 yr (with units g cm^{-2}). The plots on the left are the $0.1 M_{\odot}$ disc and on the right are the $0.07 M_{\odot}$. The top two plots are of the planets initially at 40 AU and the bottom two are for the planets initially at 80 AU. There are many similarities between the discs with the planets with similar initial orbital radii although the disc in the top left shows the most defined wakes of all four of the runs at this stage.

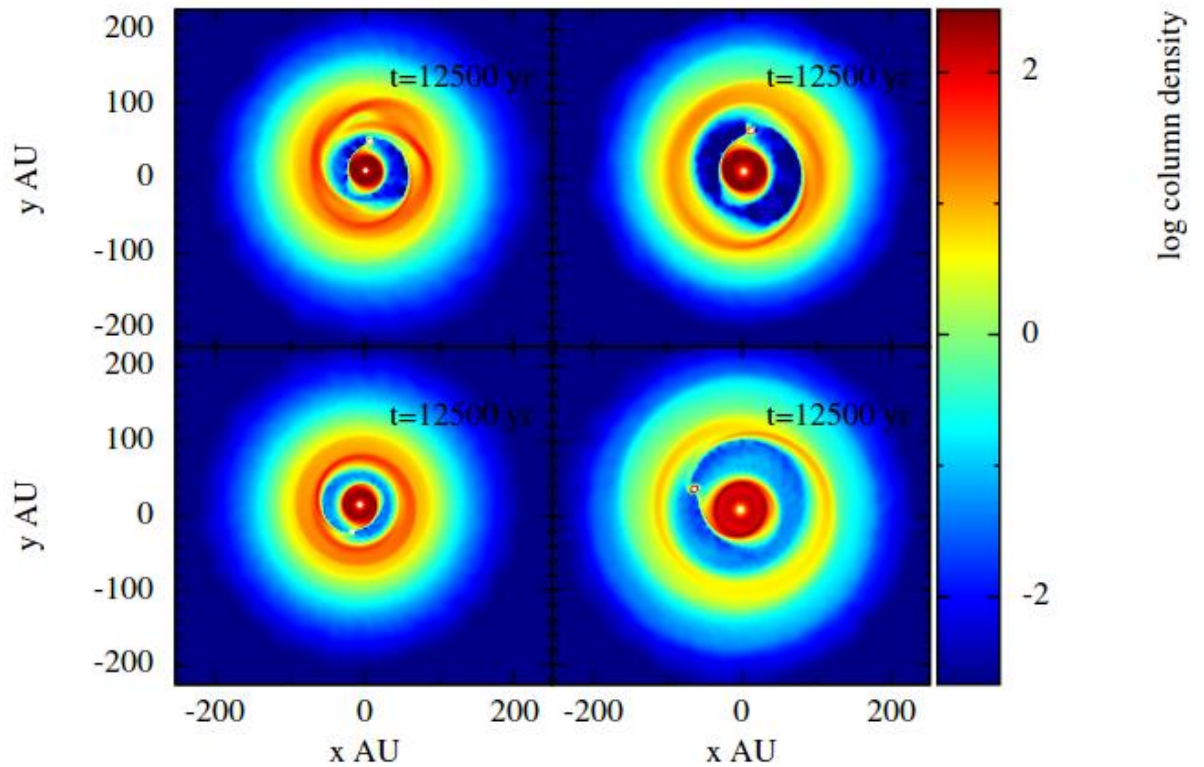


Figure 5.18: The four simulations after 12,500 yr (surface density in units g cm^{-2}). The plots on the left are the $0.1 M_{\odot}$ disc and on the right are the $0.07 M_{\odot}$. The top two plots are of the planets initially at 40 AU and the bottom two are for the planets initially at 80 AU. Gaps are starting to form along the orbits of the planets. In the plots of planets initially at 40 AU the weak outline of spiral arms can be seen.

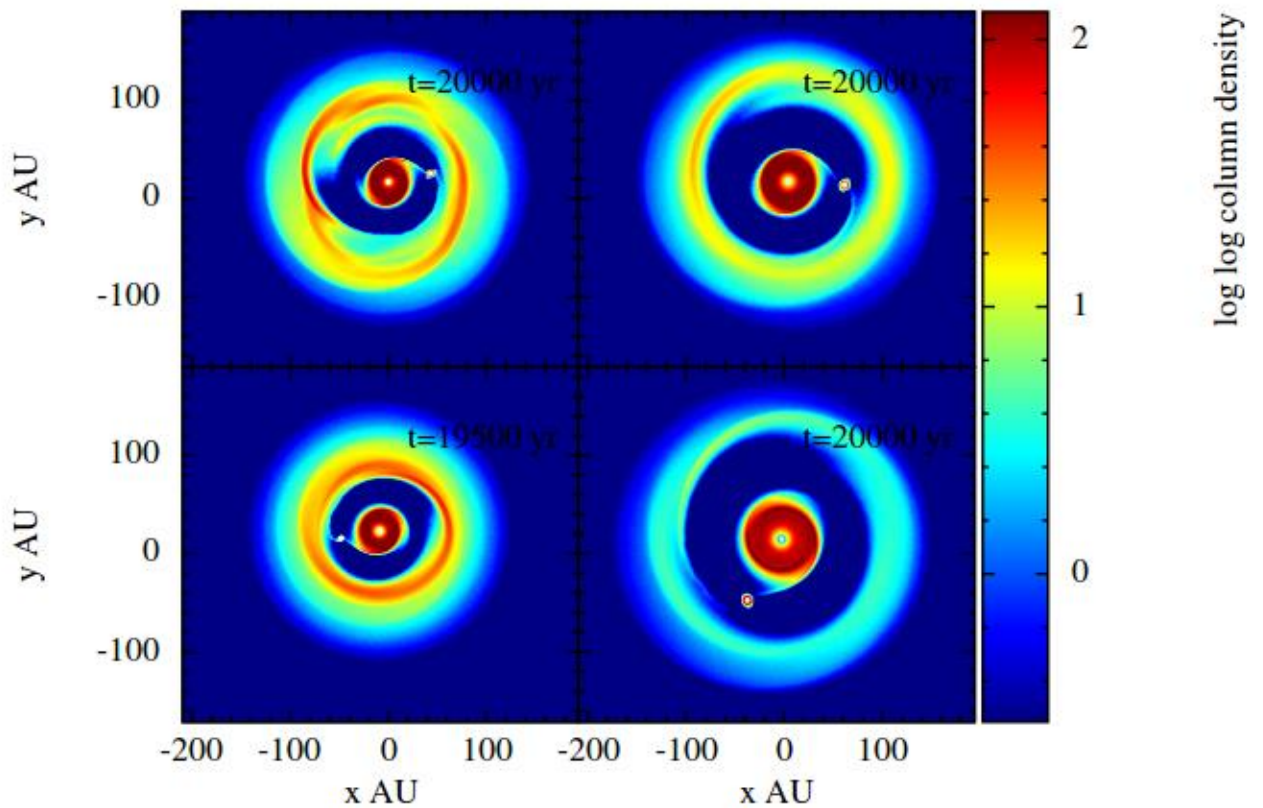


Figure 5.19: The four simulations after 20,000 yr (surface density in units g cm^{-2}). The plots on the left are the $0.1 M_{\odot}$ disc and on the right are the $0.07 M_{\odot}$. The top two plots are of the planets initially at 40 AU and the bottom two are for the planets initially at 80 AU. Gaps are now fully formed and there is a significant difference between them. The higher mass disc plots show more structure within the disc and the lower mass discs show less pronounced dense regions.

The semi-major axes (Figure 5.20 and Table 5.2) of the two planets with an initial orbital radius of 80 AU follow a very similar pattern of migration. However, both the rate of migration and the decrease in radius of the Run2 planet is greater than that of the Run4 planet. The 0.1 M_{\odot} disc will be denser than the 0.07 M_{\odot} disc as there is more mass in the same disc volume. This allows a better transfer of angular momentum through the disc for the Run2 planet and also will cause an increased torque on the inner edge of the gap compared to the Run4 planet. Both planets stabilise and very slowly start to migrate outwards from around 3 kyr to the end of the simulations. The planets initially at 40 AU do not show a similar pattern to each other (or to the planets initially at 80 AU.) The migration of the Run3 planet is minimal; however, the migration of the Run4 planet is erratic, initially showing a relatively quick inward migration before migrating outwards beyond its original orbit (shown in Figure 5.20 in red).

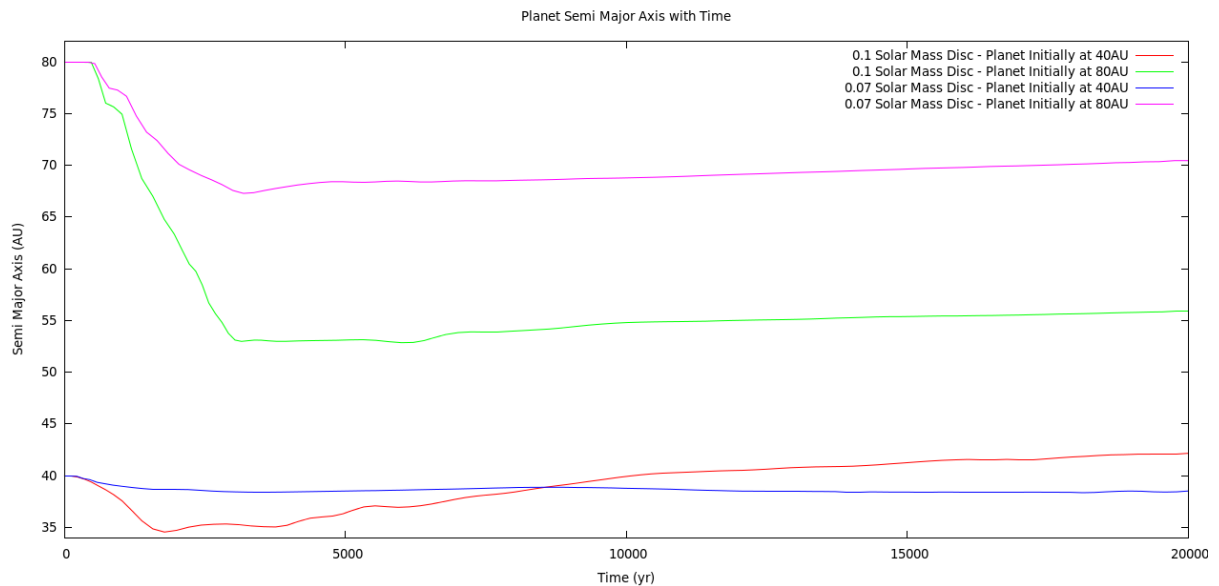


Figure 5.20: A comparison of all four planets' semi major axes over 20 kyr. All planets show initial inward migration, as they open up a gap, and all but the run3 planet show gradual outward migration over the remainder of the simulation. (Colours: Run1 → Red, Run2 → Green, Run3 → blue, Run4 → Purple).

Time (yr)	1000	2000	3000	4000	6000	8000	15000	17000
	α_1 (AU)	α_2 (AU)	α_3 (AU)	α_4 (AU)	α_5 (AU)	α_6 (AU)	α_7 (AU)	α_8 (AU)
Run1	37.6	34.9	35.5	34.9	37.1	38.3	41.2	41.6
Run2	75.7	63.8	52.9	53.1	52.7	53.9	55.4	55.5
Run3	38.9	38.7	38.4	38.4	38.6	38.9	38.4	38.4
Run4	77.3	69.8	67.1	68.2	68.6	68.6	69.6	70.0

Table 5.2: The semi-major axis, α , of the planets in the four different runs at set time intervals throughout the 20 kyr evolution of the disc. The Run1 planet shows an overall trend towards outward migration with the semi major axis of this planet being greater at the end of the simulation that it was at the start of the run. All other runs show overall inward migration. However, both Run2 and Run4 show slight outward migration after 6000 yr.

The eccentricity of all four planets increases over time (Figure 5.21). The Run1 planet shows the greatest eccentricity. The spiral arms consist of regions of relatively high density which form due to the massive nature of the disc. The variation between these high density and lower density regions (the regions of the disc which follow the general density profile) will be greatest at smaller radii from the centre of the disc which means that the Run1 planet will be most strongly influenced by these regions and their gravitational pull. As the planet interacts with the spiral arms of the disc its orbit will be pulled into a more elliptical shape.

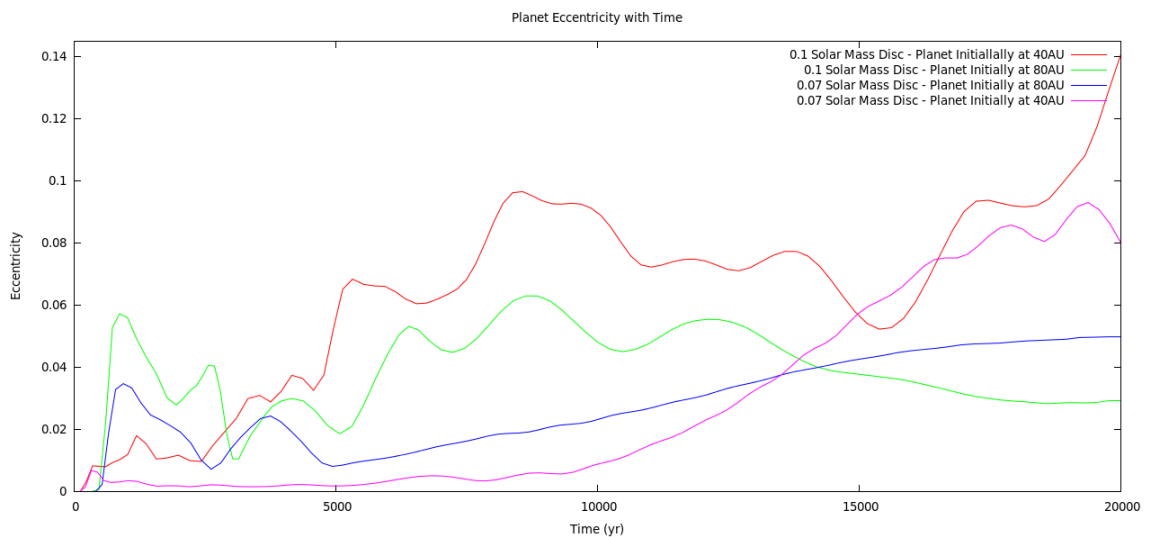


Figure 5.21: The eccentricities of all four planets over the course of the simulations. The two planets initially at 80 AU (shown here in blue and green) show the least change in eccentricity with the Run1 planet (shown in red) showing the greatest increase in orbital eccentricity. Despite this seemingly large increases, these values are very low and represent a near circular orbit.

As we would expect the planets placed within the 0.1 M_{\odot} disc show the greatest mass increase (Figure 5.22); over the course of 20 kyr their mass becomes 26 times its original value. Due to the disc being more massive the planet can accrete more gas during each orbit. The planets within the 0.07- M_{\odot} disc show a smaller increase in mass as the disc mass is smaller. The final masses of the planets are shown in Table 5.3. When we compare the final masses, we see that the only two planets showing similar masses are the Run2 and the Run4 planets.

The overall pattern of mass increase (Figure 5.22) is similar for these two planets and as expected the planet within the 0.1 M_{\odot} disc has a larger mass after 20 kyr than the planet within the 0.07 M_{\odot} disc simply due to more material being available to accrete onto the planet. Whilst most planets have a smooth increase in mass with the largest increase happening at the beginning of each run, the Run1 planet has sections of exceptionally quick increase in mass (this is especially clear at around 5,000 yr – Figure 5.22). The amount of migration which the Run1 planet experiences would not lead to such a large increase in mass if it were not for the regions of relatively very high density it interacts with.

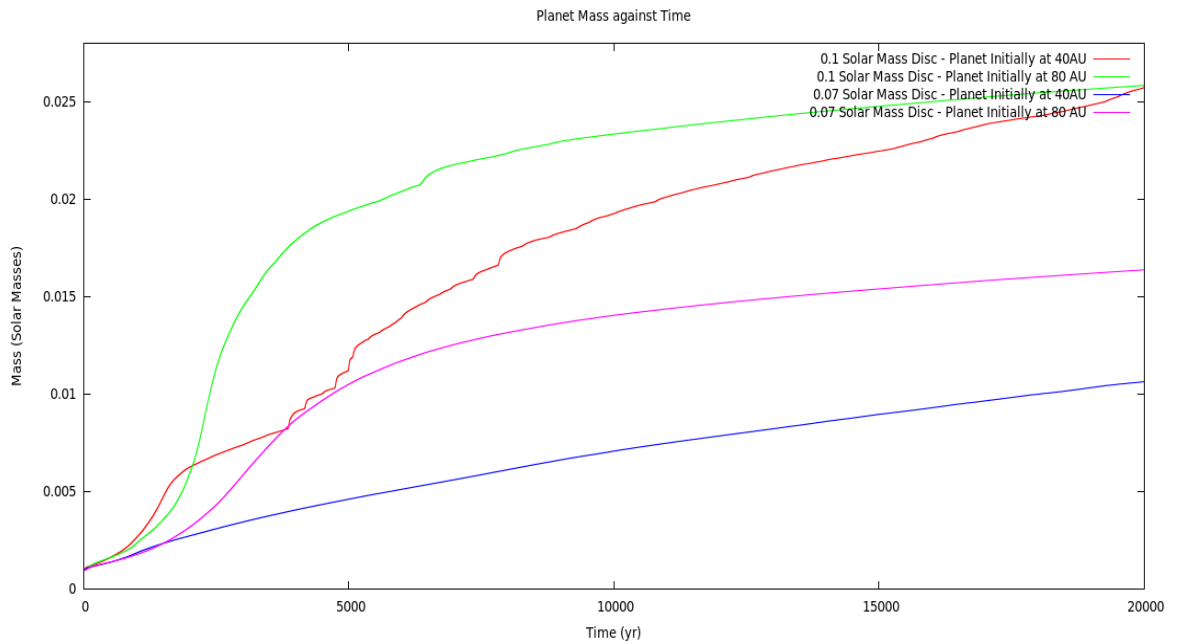


Figure 5.22: The mass of all 4 planets increases markedly throughout the simulation. The two planets initially at 80AU show a similar pattern to their mass increase, with the greatest rate of change being during their migration phase. All planets except that in Run1 have a similar mass-gradient from around 10 kyr, indicating that the accretion rates of gas onto them are similar. The Run1 planet is likely different due to it having the greatest interaction with its own wakes in the more massive of the two discs.

The masses of many of these planets by the end of the simulation suggest that they may be massive enough to be considered brown dwarfs. Runs 1, 2 and 4 “planets” all have masses above 13 M_J suggesting that they would be capable of deuterium fusion (The IAU considers an object with a mass above the limiting mass for thermonuclear fusion of deuterium to be a brown dwarf). Above about $0.08M_{\odot}$ the object can fuse hydrogen and is considered a star. Table 5.3 shows the final masses of the planets of all four runs.

	$M_{\text{final}} (M_J)$
run1	25
run2	26
run3	10
run4	16

Table 5.3: The final masses of the four planets it is purely coincidental that the two planets in run1 and run2 have such similar final mass values. In figure 5.22 these two runs appear to end at the same value however using the data directly it can be seen that there is a difference of around $1M_J$ (to two significant figures) between them.

The accretion rates of all four planets (Figure 5.23) show a similar initial pattern of a large peak followed by lower accretion rates for the rest of the simulations. The planets that migrate the most show the highest amounts of accretion during their phases of migration. Once again the exception to this rule is the Run1 planet which has a very erratic pattern of accretion. These

peaks occur at regular intervals in line with the orbital period of the planet. As the Run1 planet orbits it will regularly interact with the spiral arms that have formed in the disc. This also takes place in the Run3 planet's orbit but as the mass of the disc is much lower the spiral arms are considerably less defined, so they produce a weaker effect (Figure 5.23).

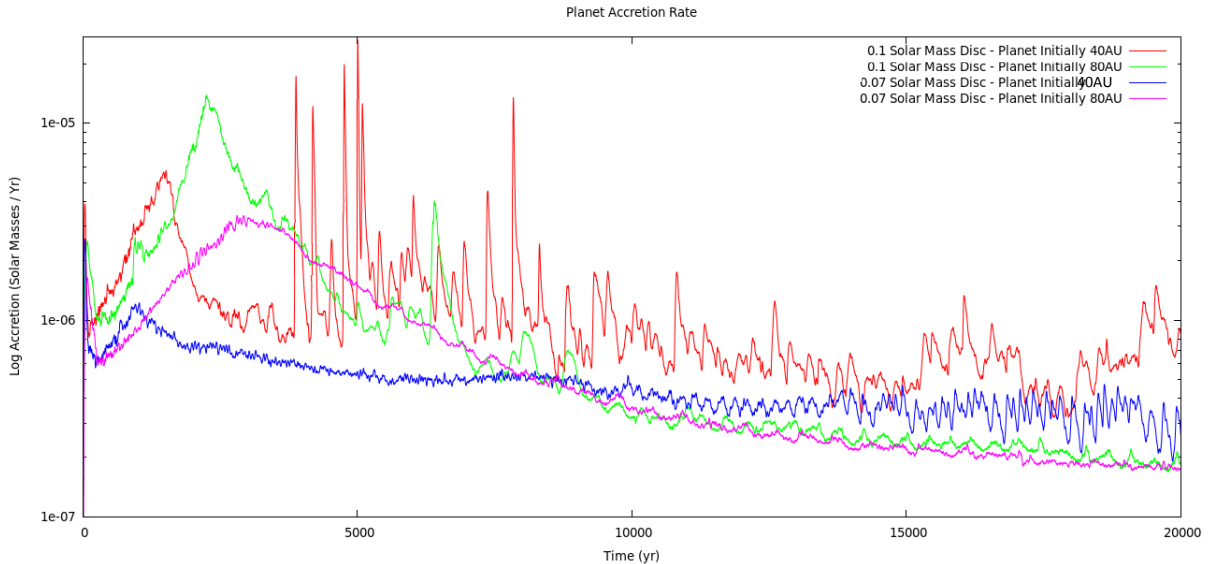


Figure 5.23: The mass of the disc and the initial radius of the planet has a very marked difference on the accretion rates of the planets. Despite all having peaks within 5,000 yr, due to their initial migration and gap opening, the accretion patterns of the planets are very different.

The accretion onto the central star in the four simulations (Figure 5.24) shows a very similar pattern between the two discs. In the case of both discs with planets initially at 40 AU the accretion rate onto the star is greater than it is in the case of the discs with the planets initially at 80 AU. This is because the relatively closer orbits drive accretion onto the star. The planets at 80 AU have far less influence over the material at the centre of the disc and therefore do not drive as much material towards the star.

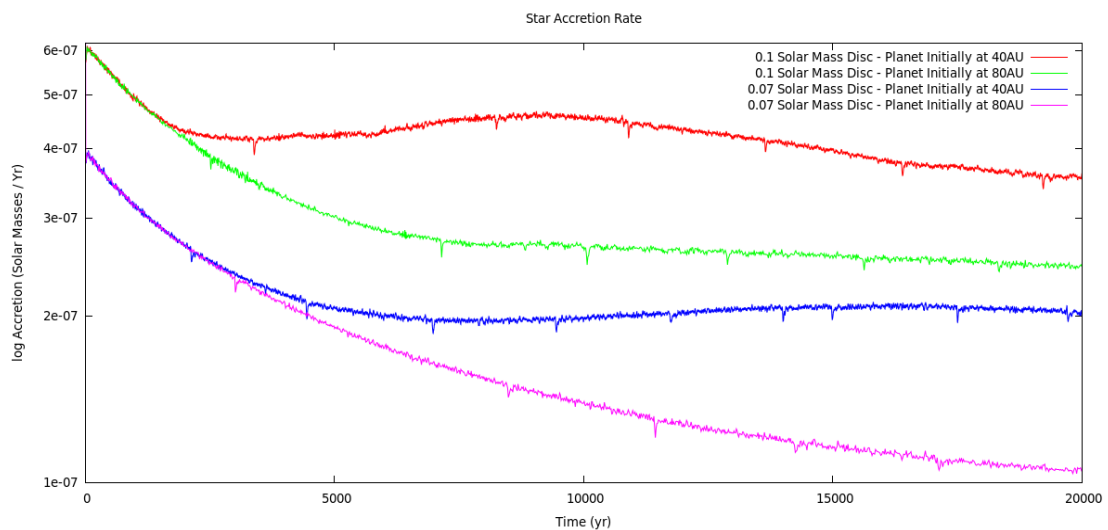


Figure 5.24: The accretion rate onto the star for all four simulations. The rates of accretion for the star in the lower mass disc (shown in purple and blue) are less than those in the higher mass disc (shown in red and green). This is simply due to less material being available for accretion in the lower mass disc. In both of the discs with the smaller orbital radius planet, accretion onto the star is greater than in the discs with a more distant planet and the planet cannot drive accretion from such distances.

Comparing the migration timescales (Table 5.4) and the rates of migration (Table 5.6) for each of the four runs shows that initially the migration is inwards but after a gap is opened up is mostly outwards. However, only in one case does this lead to a final orbital radius greater than the initial orbital radius. Run2 shows the most rapid migration which takes place right at the start of the run (between 1 and 2 kyr) at a rate of approximately 0.12 AU / yr.

	τ_1 (yr)	τ_2 (yr)	τ_3 (yr)	τ_4 (yr)
Run1	1×10^4	5×10^4	-6×10^4	-2×10^5
Run2	6×10^3	-3×10^5	-9×10^4	-7×10^5
Run3	2×10^5	-7×10^6	-3×10^5	-2×10^7
Run4	1×10^4	-6×10^4	-7×10^6	-4×10^5

Table 5.4: The migration timescales at the times listed in Table 5.3 of the four planets show that the migration is mostly outwards after an initial burst of inward migration. Inward migration is shown in green and outward migration is shown in red. These are the migration timescales of each of the planets taken at the same four times after the initial 2000 yr of the run. This is done so the planet and disc are settled into their orbit and the sudden, very high accretion rates caused by the planet being placed into a fully formed disc aren't taken into account.

	Rate of migration AU / yr						
Run1	3×10^{-3}	-6×10^{-4}	7×10^{-4}	-1×10^{-3}	-6×10^{-4}	-4×10^{-4}	-2×10^{-4}
Run2	1×10^{-2}	2×10^{-2}	-2×10^{-4}	2×10^{-4}	-6×10^{-4}	-2×10^{-4}	-8×10^{-5}
Run3	2×10^{-4}	3×10^{-4}	-6×10^{-6}	-9×10^{-5}	-1×10^{-4}	6×10^{-5}	-3×10^{-6}
Run4	8×10^{-3}	3×10^{-3}	-1×10^{-3}	-2×10^{-4}	-1×10^{-5}	-1×10^{-4}	-2×10^{-4}

Table 5.5: The rates of migration at the times listed in Table 5.3 for each of the runs shows both inward (shown in green) and outward (shown in red) migration throughout the simulation. These rates of migration are calculated by dividing the change in semi-major axis between two times by the amount of time that has passed. Each of the migration rates in the table above are averages taken over 1000 yr timeframe. The minus sign simply indicates the direction of migration is not inwards. Initially Run2 shows the highest rate of migration, moving inwards at a rate of 0.01 AU per year.

5.5 Comparisons with other studies

The findings in all four of our runs are in line with findings of previous studies however this is the first time such studies have been carried out using the radiative transfer method in massive discs. Migration timescales are similar to those of previous studies, with values between 6×10^3 and 2×10^5 initially. Studies by Stamatellos (2015), Baruteau et al. (2011) and Michael et al. (2011) found initial migration time scales to be in the order of $\sim 10^4$ years. We find that our planets initially migrate inwards as predicted by previous studies with a migration timescale between 1.7 and 2.6×10^4 yr as in Stamatellos 2015 where radiative transfer is included (as in this study). In contrast with previous studies (e.g. Michael et al. 2011, Baruteau et al. 2011) we find that the planet is able to open gap and the migration slows down and even reverses to an

outward migration. Therefore, planets forming early on are able to survive on a wide orbits. However, many of them accrete enough mass to become brown dwarfs.

5.6 Summary

After running four simulations we found that planets will show the greatest inwards migration during the first few kyr. In all cases this migration slows and reverses leading to a steady outward migration for the rest of the run. Initial migration timescales were in the same order as those found in previous studies $\sim 10^4$ yr, however after around 5 kyr these migration timescales became negative ie the migration is outwards. We also see a significant mass increase of all planets, with most becoming brown dwarfs of mass greater than $13M_J$.

Chapter 6

Conclusions

We used SPH to study giant planet migration in massive protostellar discs. Our main goal was to study the migration of giant planets that are initially on wide orbits (~ 50 AU) in newly formed protostellar discs. Such planets may have formed by disc fragmentation very early after the formation of the disc. At this early phase protostellar discs are relatively massive ($\sim 0.1 - 0.3 M_{\odot}$) and therefore are close to being gravitationally unstable (e.g. Stamatellos et al. 2011).

We set up the disc by balancing vertically to the disc midplane the thermal pressure of the disc with the gravity of the star and the disc self-gravity. The disc is then evolved using the SEREN Smoothed Particle Hydrodynamics code for three orbits of the outer edge of the disc. This creates a more random and natural distribution of SPH particles. A second sink particle is then added to act as the planet and the disc is then further evolved using SEREN. From this we can calculate the migration profile of the planets.

We tested our code by comparing our findings to those of previous studies (Ayliffe & Bate 2010). We then compared the migration timescales of giant planets in low-mass discs with the ones found by AB2010 for locally isothermal discs and for discs where the radiative transfer is taken into account. The values which are calculated in our runs are within the same range as those calculated in AB2010, suggesting that our code is suitable for use with this study.

We studied the giant planet migration in massive discs and the effect of disc mass and planet initial orbital radius, by comparing two initial orbital radii and then two different disc masses to see what affect this has on the final mass, location and migration timescale of the planets.

All planets showed rapid initial inward migration. At this point the planets were completely surrounded by the disc and underwent Type I migration inwards. In all cases, a gap is opened due to the planet accreting gas material within its orbit. Once this gap is opened, we see a very slow outward migration. Therefore, planets are able to survive on a wide orbits but they may accrete enough mass to become brown dwarfs. This is in contrast with previous studies that find that planets do not open up a gap and migration does not stop.

As this study only ran simulations for 20 kyr, we cannot say that this outward migration would continue for the rest of the life span of the disc, however this outward migration could help to explain the existence of giant planets in very wide orbits ~ 100 AU, which are currently being observed in our Galaxy (e.g. Bailey et al. 2014; Rameau et al. 2013; Galicher et al. 2014; Kraus et al. 2014).

We find that a planet initially at a large orbital radius will migrate rapidly inwards due to Type I migration and direct interaction with the disc. The more massive the disc, the more rapidly the planet migrates inwards. In this study, the planets initially at a radius of 80 AU undergo the highest rate of migration whilst the planet, initially at 40 AU in the lower mass disc, undergoes very little inwards migration. In comparison the 40 AU initial orbital radius planet in the $0.1 M_{\odot}$ disc shows a rapid inward migration, followed by an outward migration which leaves it at a final orbit greater than its initial orbit; an overall outward migration.

REFERENCES

Armitage, 2007, arXiv:1509.06382 [astro-ph.SR]

Ayliffe B. A., Bate M. R., 2010, MNRAS, 408, 876

Ayliffe, B. A., & Bate, M. R. 2009, MNRAS, 393, 49

Barnes J, Hut P., Nature, 324 (1986) 446-449

Baruteau C., Meru F., & Paardekooper S. J., 2011, MNRAS, 416, 1971

Bate M. R., Bonnell I. A., Price N. M., 1995, MNRAS, 277, 362

Bate M. R., Lubow S. H., Ogilvie G. I., & Miller K. A. 2003, MNRAS, 341, 213

Batygin K., & Brown M. E., 2016, AJ, 151, 22

Boss A. P., 2011, arXiv:1107.0294 [astro-ph.EP]

Boss A. P., 1997, Science, 276, 1836

Garaud, P., Meru, F., Galvagni, M., & Olczak, C. 2013 ApJ, 764, 146

Goldreich P., Tremaine S., 1980, ApJ, 241, 425

Goldreich, P., & Ward, W. R. 1973, ApJ, 183, 1051

Goodman J., Rafikov R. R., 2001, ApJ, 552:793-802

Gomes R., Levison H.F., Tsiganis K., & Morbidelli A., 2005, *Nature*, 435, 466

Hartman J. D., Bayliss D., Brahm R., G. Á. Bakos, L. Mancini, A. Jordán, K. Penev, M. Rabus, G. Zhou, R. P. Butler, N. Espinoza, M. de Val-Borro, W. Bhatti, Z. Csubry, S. Ciceri, T. Henning, B. Schmidt, P. Arriagada, S. Shectman, J. Crane, I. Thompson, V. Suc, B. Csák, T. G. Tan, R. W. Noyes, J. Lázár, I. Papp, P. Sári, 2014, *AJ*, 147, 128

Hubber, D. A., Batty, C. P., Mcleod, A., & Whitworth, A. P. 2011, *Astronomy & Astrophysics*, 529, A27

Lin, D. N. C, Bodenheimer, P, Richardson, D. C., 1996, *Nature*, Volume 380, Issue 6575, pp. 606-607

Martin T. J., Pearce F.R., Thomas P. A., 1993, arXiv:astro-ph/9310024

Matsuo T., Shibai H., Ootsubo T., 2007, *ApJ* 662:1282-1292

Michael, S., Durisen, R. H., & Boley, A. C. 2011, *ApJ*, 737, L42

Monaghan, J. J., Lattanzio, J. C., 1985, *Astronomy and Astrophysics*, vol. 149, p. 135-143

Monaghan J. J., 1992, *ARA&A*, 30, 543

Mustill A. J., Raymond S.N., Davies, M. B., 2016, *MNRAS*, 460, L109

Pollack, J. B., Hubickyj, O., Bodenheimer, P., Lissauer, J. J., Podolak, M., & Greenzweig, Y. 1996, *Icarus*, 124, 62

Rice W. K. M., Lodato G., Pringle J. E., Armitage P. J., Bonnell I. A., 2004, *MNRAS*, 355, 543

Semenov, D., Henning, T., Helling, C., Ilgner, M., & Sedlmayr, E. 2003, *A&A*, 410, 611

Stamatellos, D., & Whitworth, A. P. 2009a, *MNRAS*, 392, 413 —. 2009b, *MNRAS*, 400, 1563

Stamatellos D., 2013, European Physical Journal Web of Conferences, 47, 08001

Stamatellos D., 2015, *apjl*, 810, L11

Stamatellos, D., Whitworth, A. P., & Hubber, D. A. 2011, *ApJ*, 730, 32

Stamatellos D., Whitworth A. P., Bisbas T., Goodwin S., 2007b, *A&A*, 475, 37

Tanaka H., Takeuchi T., Ward W. R., 2002, *ApJ*, 565, 1257

Toomre A., 1964, *ApJ*, 139, 1217

Ward, W. R. 1997, *Icarus*, 126, 261

Weidenschilling S. J., 1977, *MNRAS*, 180, 57

Wolk & Walter, 1996, *aj*, 111, 2066